UNIVERSITY OF THESSALY

POLYTECHNIC SCHOOL

DEPARTMENT OF MECHANICAL ENGINEERING

LABORATORY OF MATERIALS

Diploma Thesis

Investigation of Stress-Oriented Hydrogen-Induced Cracking (SOHIC) in an Amine Absorber Column of an Oil Refinery

By

Papageorgiou Pantelis-Panagiotis

Supervisor:

Dr. Helen Kamoutsi

Submitted for the Partial Fulfillment

of the requirements for the degree of

Diploma in Mechanical Engineering

Volos

2019

Certified by the members of the Thesis Committee:

First examiner	Dr. Helen Kamoutsi
(Supervisor)	Lab Teaching Staff, Department of Mechanical Engineering, University of Thessaly
Second Examiner	Dr. Nikolaos Aravas Professor, Department of Mechanical Engineering, University of Thessaly
Third Examiner	Dr. Alexandros Kermanidis Assistant Professor, Department of Mechanical Engineering, University of Thessaly

Acknowledgments

This project is accomplished in the scope of partial fulfilment of the requirements for the degree of Diploma in Mechanical Engineering at University of Thessaly.

For the completion of this Thesis, I would like to thank my thesis supervisor, Dr. Helen Kamoutsi whose expertise, valuable suggestions, comments, guidance and patience further considerably my knowledge, as well as for the support over this semester.

Furthermore, very special thanks go to Professor Nikolaos Aravas and Assistant Professor Alexandros Kermanidis for accepting to be the referees of this work.

I would also like to express my great appreciation Professor Nikolaos Aravas, for his important guidance at appendix A and Associate Professor Kyriaki Polychronopoulou for conducting the SEM experiments.

I would also like to thank Professor Gregory Haidemenopoulos for giving me the opportunity in the current Thesis to deal with such an interesting topic.

Last but not least, special recognition goes to my family and all my friends for their continuous support and encouragement during this study.

Pantelis-Panagiotis Papageorgiou

Abstract

Stress oriented hydrogen induced cracking (SOHIC) of an amine absorber column made of a HIC-resistant steel and operating under wet H_2S service was investigated. SOHIC was not related to welds in the column and evolved in two steps: initiation of HIC cracks in the rolling plane and through-thickness linking of the HIC cracks. Both the original HIC cracks as well as the linking cracks propagated with a cleavage mechanism. The key factors identified were periods with high hydrogen charging conditions, manifested by high H_2S/amine ratio, and stress triaxiality, imposed by the relatively large thickness of the plate. In addition, the mechanical properties of the steel away from cracked regions were unaffected, indicating the localized nature of SOHIC.

Table of contents

List of Figures

List of tables

1 Introduction

1.1 Description of the problem

Amine absorber columns in oil refineries are columns which are used to remove acid gas from natural gas or natural gas liquid (NGL). The most common acid gas was hydrogen sulfide (H_2S) and carbon dioxide (CO_2), where a down flowing amine solution absorbs H_2S from the up flowing sour gas stream. The H_2S-rich amine solution, when exiting the absorber, is routed to a regenerator to produce an H_2S-lean amine that is recycled for use in the absorber. This process is called sweetening process cause the pH increasing of the stream [1].

Under specific operation conditions, where the ratio of H_2S/amine is high, H_2S corrosion of the steel shell can take place, producing hydrogen, which can then enter the steel and cause hydrogen blistering and hydrogen-induced cracking. According to API 571 [2], it is atomic hydrogen that enters the material and diffuses through the lattice. The hydrogen is then concentrated to various microstructural sites, such as interfaces between the matrix and inclusions or interfaces between the matrix and other phases. The local pressure increases and decohesion takes place, generating internal blistering or so-called hydrogen-induced cracking (HIC). In most cases HIC cracks are oriented parallel to the rolling plane. Under the action of applied or residual stresses the HIC cracks arrange in a vertically (through thickness) stacked array. Subsequently the array is joined by cracks between the individual HIC cracks, which run perpendicular to the main applied stress. The interconnected HIC cracks, which run through the thickness of the plate form a significant through-thickness crack. This cracking is classified as stress-oriented hydrogen-induced cracking (SOHIC). As mentioned above, hydrogen is produced by a corrosion reaction, such as when steel is exposed to wet H_2S service.

Hydrogen damage in wet H_2S environments is classified as blistering, hydrogen induced cracking, stepwise cracking [3], stress oriented hydrogen induced cracking and sulfide stress cracking in API 571 recommended practice[2]while the assessment of hydrogen damage is performed in accordance with API 579 [4] following the work of Buchheim et al. [5] on the development of a fitness-for-service rules for the assessment of HIC and SOHIC damage. While hydrogen blistering and HIC is a frequent problem when steel operates in wet H_2S service, SOHIC is a rather rare phenomenon and when occurring is mostly associated with residual stresses at welds. SOHIC in pipelines and pressure vessels has been thoroughly reviewed by Pargeter [6]. Most of the case studies reported, associated with SOHIC, are related with SOHIC at welds and concern mostly pipelines. There is only one case of SOHIC in an amine absorber column, reported by McHenry et al. [7] regarding the Chicago refinery incident in 1984. Even in this case, SOHIC originated from the HAZ of a repair weld, which did not receive a stress relieving post weld heat treatment. Following the Chicago refinery incident, the Occupational Safety and Health Administration (OSHA) of the Department of Labor issued, in 1986, a memorandum [7] stating, among others, that

in a survey of similar refinery vessels and associated equipment, conducted by the National Association of Corrosion Engineers (NACE), approximately 60% of 24 amine absorbers evaluated, exhibited cracking. In addition, 12 of 14 monoethanolamine (MEA) units and three of five diethanolamine (DEA) units exhibited cracking. Sixteen instances of cracking were reported in associated equipment (i.e., regeneration units and piping) exposed to a chemically similar environment. Additionally, a similar survey by the Japan Petroleum Institute indicated that cracking had occurred in 72% of the amine gas treatment facilities, which had responded to the survey.

As mentioned above, most failure cases involving SOHIC refer to welded piping, such as the work by Anezi et al. [8] in spiral welded pipes. The effects of loading and microstructure have been discussed by Kobayashi et al. [9] as well as by Koh et al. [10], while the effects of heat treatment on SOHIC of pressure vessel steels have been discussed by Tsuchida et al. [11]. Most reported results refer to HIC, as the work of Findley et al. [12] on the mechanism of HIC in pipeline steels and the work of Gan et al. [13] on hydrogen trapping in H_2S environments. In-situ observation of HIC propagation is reported by Fujishiro et al. [14], while corrosion-induced microcracking in H_2S environments has been discussed by Okonkwo et al. [15]. A recent review of HIC in pipelines and pressure vessel steels is presented by Ghosh et al. [16]. The reported cases of SOHIC failures in pressure vessels are limited and mostly associated with welds. The present case refers to SOHIC in the base plate of a pressure vessel, away from welds. This is a rare case and it is, therefore, very important to investigate the conditions and contributing factors of this type of damage.

A decommissioned amine absorber column, which exhibited hydrogen blistering in the internal wall, was made available for study. The aim of the present work is to investigate the underlying SOHIC damage and to identify the contributing factors that led to cracking.

Parts of this thesis are contained in paper which was published in MDPI journal at 24 August 2018 and was presented at the ICEAF V 5th International Conference of Engineering Against Failure 20 - 22 June 2018 Chios Island, Greece.

1.2 Thesis objectives

In view of the above considerations, the present thesis tries to further elucidate the failure mechanisms that occurring in wet H_2S service. Also, to explain the operation condition that led to this failure.

1.3 Thesis methodology

Research was focused on steel SA-516 Gr 60 HIC resistant. The experimental procedures involved the following actions:

1) Ultrasonic Test
2) Tensile Test
3) Charpy -V-Notch
4) Hardness Test Vickers

5) Fractography

1.4 Thesis outline

The thesis outline is as follows:

1. Introduction
2. Literature review
3. Experimental procedures
4. Results and Discussion
5. Conclusions

2 Literature Review

2.1 Amine absorber column

2.1.1 Operating conditions

The removal of acid gas such as hydrogen sulfide (H_2S) and carbon dioxide (CO_2) from natural gas or is usually necessary in gas plants and oil refineries. The absorption process using aqueous solutions of alkanolamines is often used as a treatment technology. Figure 1 illustrates the process flow diagram of a typical amine-sweetening unit. The system consists of two major operations: absorption and regeneration.

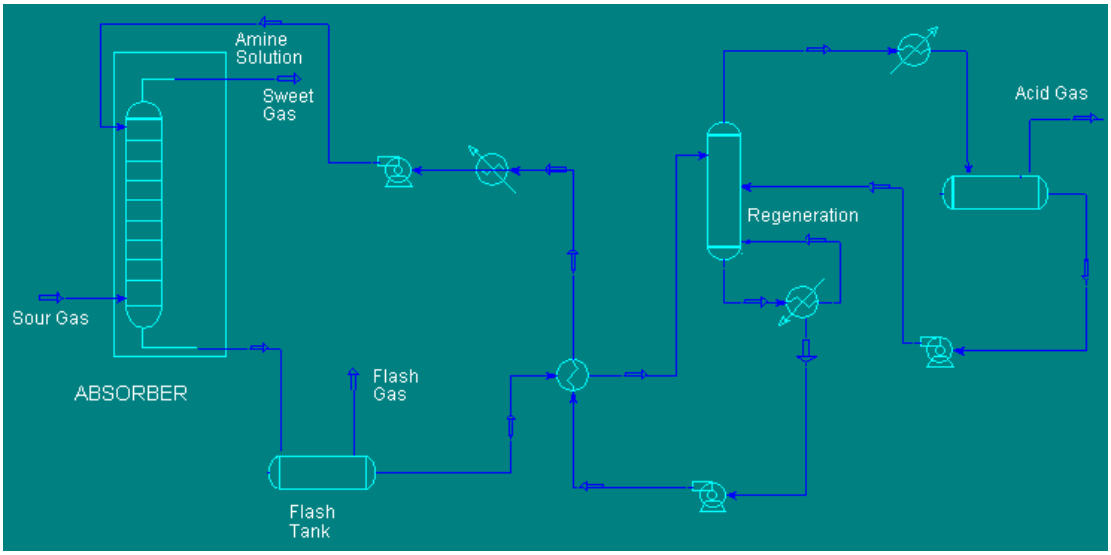

Figure 1. Amine Absorber Column [1].

A natural gas stream that contains acid gases (H_2S and/or CO_2) is introduced into an absorber column where the stream is counter-currently contacted with an amine solution. The acid gas contents are removed by chemical reactions with the amine. After treatment, the natural gas is suitable for consumer use or further chemical processing. This process is referred to as a gas sweetening process and treated gas is called sweetened gas or liquid. After the absorption process, the amine solution, (referred to as rich amine solution after selectively absorbing the acid gases) requires regeneration before it can be used to sweeten sour gas again. The regeneration column serves the function of stripping absorbed acid gases from the rich amine solution. A flash tank is usually installed at the outlet of the absorber to permit the recovery of the dissolved and entrained hydrocarbons and to reduce the hydrocarbon contents of the acid gas product. The flash gas from the flash tank and the stripped acid gas from the regenerator in amine units have the potential to emit hazardous air pollutants and volatile organic compounds. In processes for complete acid-gas removal, when the column contains enough trays or packed depth, treated gas quality is determined by phase equilibrium, [1].

The amine solution temperature entering the absorber is usually 10 to 15^{o}C higher than the inlet feed gas temperature to prevent condensation of hydrocarbon in the contactor, which can cause foaming. The inlet feed gas usually enters the absorber at 38 - 49 ^{o}C. Therefore, the typical range of lean amine solvent temperature is 46 - 57^{o}C. It is good practice for the lean amine solvent temperature not exceed 57 ^{o}C. High lean solvent temperatures can lead to poor solvent performance due to H2S equilibrium problems on the top tray of the absorber or increased solution losses due to excessive vaporization losses. The temperature of rich amine leaving the absorber will be 54.4 to 71.1°C [17].

2.2 Corrosion

A common failure at the absorber is the corrosion by H_2S service or by amine solution. At this section are listed the categories of the failure.

2.2.1 Hydrogen service

Hydrogen damage failures are classified in two categories based on the corrosion mechanism:

- Electrochemical processes arising from acid corrosion or cathodic protection at low temperature, up to 100 ^oC.
- High temperature,200 ^oC until 900 ^oC, arising from the presence of hydrogen gas at high pressure.

At the following subsection only the first category is analyzed, as in the case of the absorber studied in this thesis, the operating temperature was 70 ^oC. As discussed in the above, in the presence of aqueous solution of acids H_2S, iron corrodes according to two electrochemical reactions that occur simultaneously, a cathodic and an anodic reaction. According to, the Groysman, Kane and Zheng [18-21] the anodic reaction is:

$$Fe_{(s)} \rightarrow Fe^{2+}_{(aq)} + 2e^-$$

Which consists of the dissolution of iron in positive metallic ions (Fe^{2+}) and electrons remaining on the metal surface. These electrons concentrate on adjacent areas with higher electric potential. The cathodic reaction is:

$$H_2S + 2e^- \rightarrow 2H^+_{(aq)} + S^{2-}$$

$$2\ H^+_{(aq)} + 2e^- \rightarrow H_{2(g)}$$

Hydrogen sulfide is collecting electrons from the anodic reaction releasing hydrogen cations and sulfide anions. Also, electrons are collecting from the generated hydrogen cations and are created hydrogens in gas form. Finally, the complete reaction is:

$$Fe_{(s)} + H_2S_{(aq)} \rightarrow FeS_{(s)} + H_{2(g)}$$

Depending on the chemical composition of the alloy, H_2S concentration, temperature and pH the net reaction can create different corrosion products (iron sulfides). Some of them are:

- Iron (II) sulfide (FeS, amorphous)
- greigite (iron (II, III) sulfide, Fe3S4
- analog to magnetite Fe3O4)
- pyrrhotite (Fe1−xS, where x = 0–0.2, Fe7S8)
- troilite (FeS, crystallic)
- mackinawite (Fe1+xS, where x = 0–0.1or Fe9S8)
- marcasite (iron (II) disulfide FeS2, orthorhombic)
- pyrite (iron (II) disulfide FeS2, cubic)

If the iron sulfide concentration is low, a thin protective file is created at the surface of the steel protecting it from corrosion. If the concentration is high, the iron sulfide is more electrically potential than the iron surface and as a result corrosion reaction is accelerated.

By the above net reaction atomic hydrogen forms, which is very active and diffuses into the metallic lattice. When atomic hydrogen is concentrated, it recombines H_2, which due to its larger dimension is prohibited from entering, absorbing and diffusing into the metallic lattice. On the metal surface this recombination occurs faster than the gas phase. The ratio of rates of cathodic reduction of H^+ and formation of H_2 define the intensity of hydrogen absorption by the steel. The ions S^{2-} and HS^- accelerated the cathodic reaction of H^+ and decrease the recombination, which results in the increasing of absorption of hydrogen by metal.

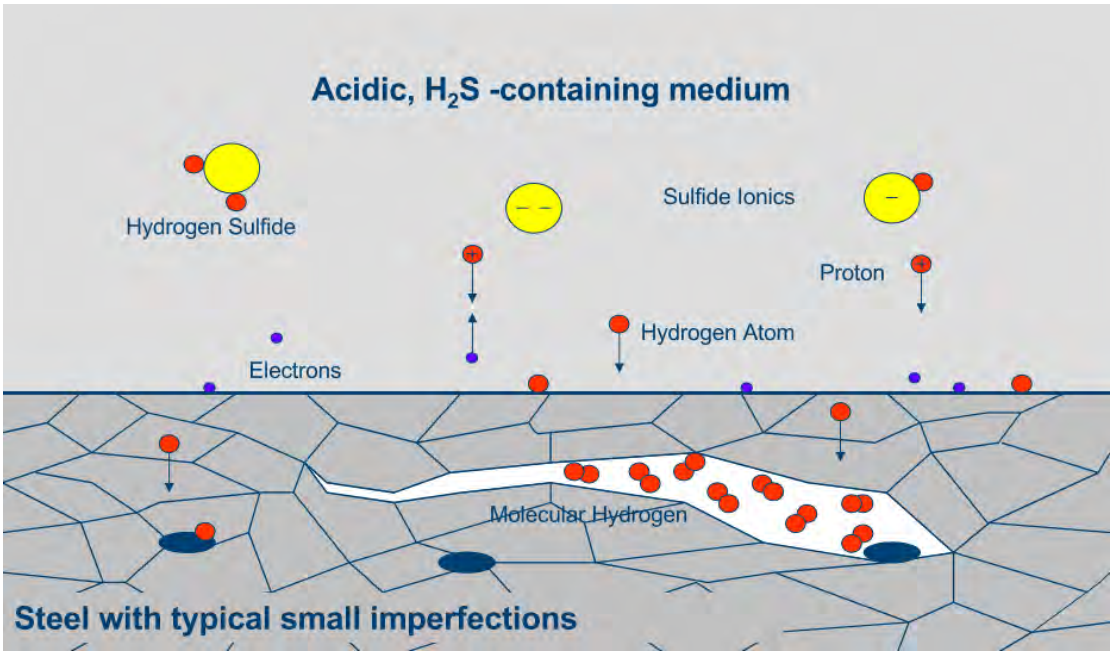

Figure 2. Steel with typical small imperfections.

Some atoms of hydrogen polarize and form H^- ions. Some other atoms and gaseous molecular hydrogen are present in equilibrium inside the steel. The accumulation positions are: micro-voids, blowholes, pores, non-metallic inclusions, cracks, accumulation of dislocations, and grain boundaries.

The microstructure of steel has significant influence on the absorption of hydrogen. Much greater hydrogen solubility occurs in austenite steel than in ferrite. The rate of hydrogen permeability is greater in perlite structure than in martensite.

The mechanical properties of steel (plasticity, ductility, toughness and tensile strength) are changed significantly when hydrogen is absorbed in the microstructure, as a result creating cracks. These cracks are classified in two categories [20].

In the first category the cracks arise without any externally applied or residual stress:

- Internal cracking.
- Stepwise cracking.
- Hydrogen induced cracking (HIC).
- Hydrogen pressure induced cracking (HPIC).

In the second category belong cracks which the failure occurs under applied or residual stresses, static or cyclic, such as:

- Stress orient hydrogen induced cracking (SOHIC).
- Sulfide stress cracking (SSC).

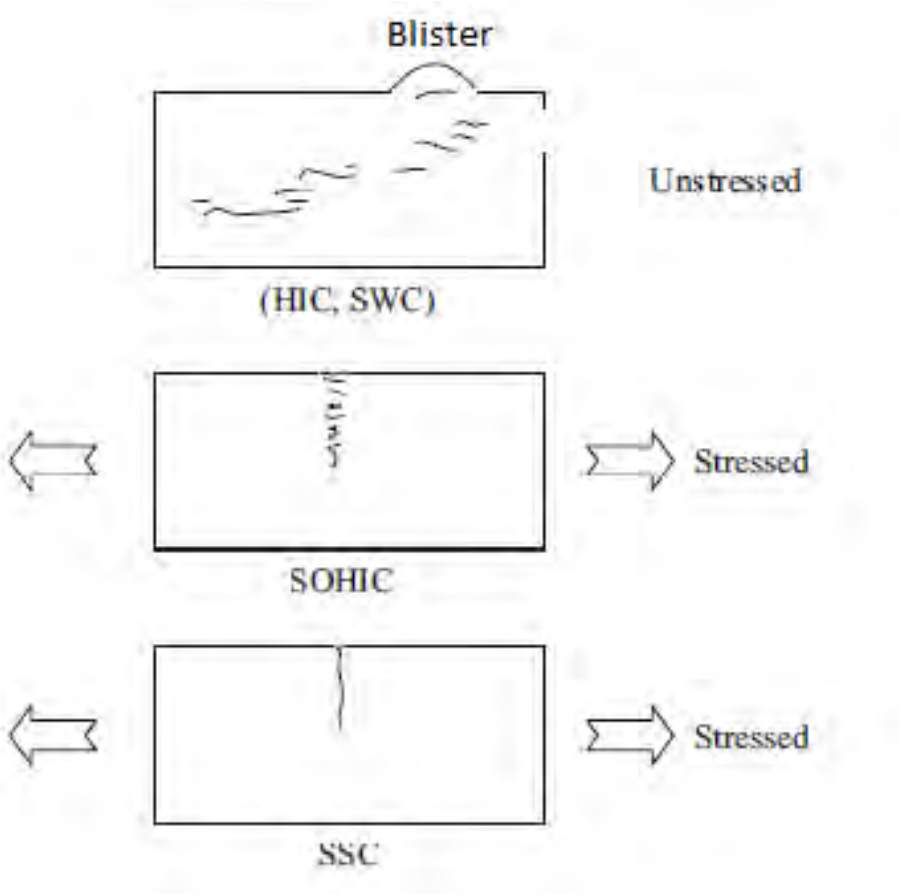

Figure 3. Kind of cracking [20].

2.2.1.1 Cracks without stress

As discussing above, the accumulation of atomic hydrogen forms molecules of hydrogen at trap sites inside the steel lattice. The rolled products, along elongated inclusions or segregated bands of microstructure, contains trap sites [3].

Hydrogen blistering: Is called the blister that become visible, from the deformation of adjacent steel, at the surface of the material. They are created by rise of pressure inside the voids in which the concentrate of molecules hydrogen is increased [3, 22, 23].

Hydrogen Induced Cracking (HIC): According the ELBOUJDAINI's paper [23], Hydrogen-induced cracking occurs in three steps:

- Formation of hydrogen atoms at the steel surface and adsorption on the surface.
- Diffusion of adsorbed hydrogen atoms into the steel substrate.
- Accumulation of hydrogen atoms at hydrogen traps, such as voids around inclusions in the steel matrix, leading to increased internal pressure and crack initiation and propagation.

They are a form of blistering in which laminating-type fissures (exfoliation) parallel to the metal surface link in the through-surface direction.

Stepwise Cracking: This type of cracking is formed by adjacent links of the hydrogen blisters and the hydrogen induced cracking. Because it grows without applied or residual stress, it increased as corrosion continues. In Figure 3, is shown the morphology of stepwise cracking [3, 22, 24].

2.2.1.2 Cracks arise from applied or residual stress.

Sulfide stress cracking (SSC): Like the others cracks, this type occurs when the hydrogen is diffused inside the steel matrix. The mainly difference with others cracks is that SSC remains in solid solution in the crystal lattice[3]. For the development of the embrittlement must applied tensile stress at the material. In Figure 3, is shown a hydrogen embrittlement by SSC.

The steels with high strength microstructure (martensite and bainite) maximize resistance to SSC. There are a lot of processes for producing these steels. Some of them is annealing normalizing, normalizing and tempering, quenching and tempering (Q&T). According to the preferred process is Q&T [20, 25]. Because she has two major benefits:

- The production of a martensitic structure in the material by balancing steel composition and the critical cooling rate to produce complete martensitic transformation.

- A fully martensitic, as quenched structure allows tempering to be conducted at higher temperatures leading to production of a high SSC resistant spheroidized carbide structure while retaining high strength.

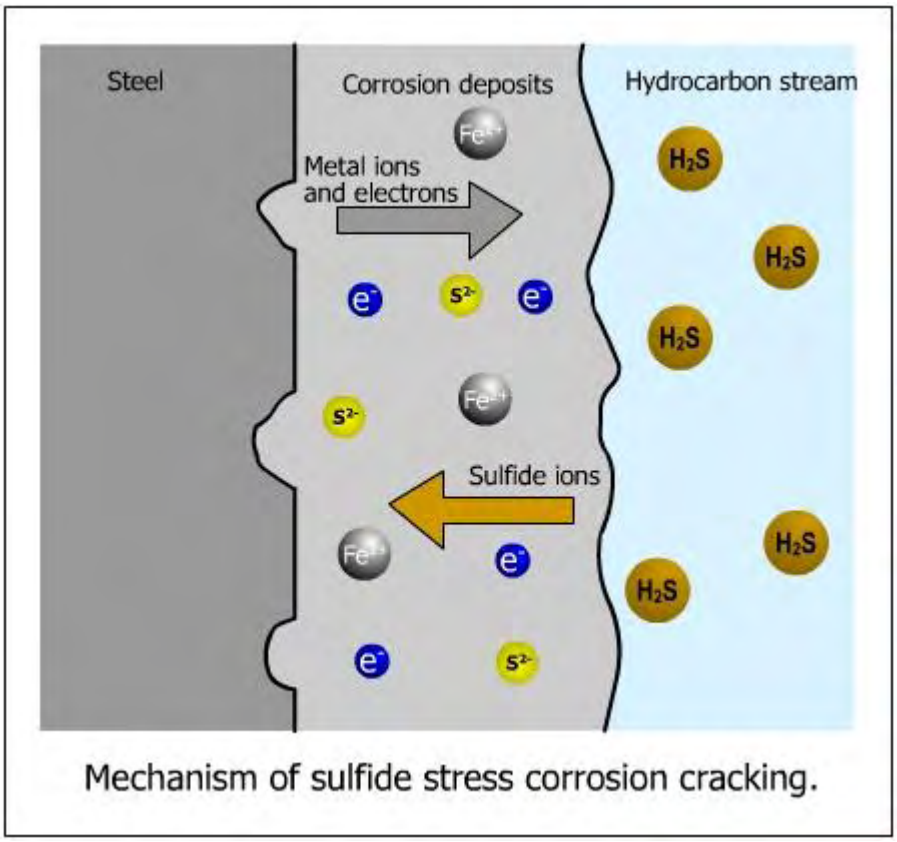

Figure 4. Mechanisms of SSC cracking

Stress oriented hydrogen induced cracking (SOHIC):

Finally, the last kind of cracks is the SOHIC. This cracking is related with SSC or Stepwise cracking. The main difference of these cracks is that the SOHIC small cracks, like as HIC, formed perpendicular at the applied or residual stress. As a result, the creation of 'ladder-like' crack. SOHIC is related to the increase triaxial stress of the molecule's hydrogen and the yield strength of the material [3, 22, 24].

2.2.2 Corrosion by amine solution.

In oil refineries aqueous amine solutions are used to avoid corrosion from acid solutions, like H_2S or CO_2. Amines are not sorely responsible for the corrosion of steel. Corrosion in oil refineries is mainly caused by acid solution and by amine degradation products. The amines that are usually used, are listed below:

- Monoethanolamine (MEA): The methanol molecule loses an H bond and attaches to the amine molecule, which also lose an H bond. The formula is CH_2OHNH_2
- Diglycolamine (DGA) and Diethanolamine (DEA): These are secondary amines, which are similar with MEA, but they have two alcohol molecules for one amine molecule. The formula is NHR_2, where are represent the alcohol radical.
- Methyldiethanolamine (MDEA) and Diisopropanolamine (DIPA): These are tertiary amines with 3 alcohol radicals to the N atoms. The formula is NR_3

In the amine solution oxidation of hydrocarbons, results in the production of contaminants (for example acid solutions, chlorides, sulfate, thiosulfate), which react with the amine producing salts (for example formate, acetate, chloride, sulfate, thiosulfate). These products are called Heat Stable Amine Salts (HSAS) or simply Heat Stable Salts (HSS). The characteristic of these products is that they cannot be destroyed under normal regenerator conditions, they cannot be recovered by heating and they must have specific concentration to avoid corrosion [20].

According to L. Beke, steel reacts with H_2S to form a layer of FeS on the surface that protects the steel from further attack. As long as the layer of FeS is intact, the overall corrosion rate is quite low. The iron sulfide layer is soft and friable. It can be worn away by high flow velocity or turbulence. High HSS content increases the viscosity and density of the amine solution. At the same time if higher amine solution circulation rates are required to circulate enough free amine to pick up the acid gas, solution velocities go up. This combination can result in erosion of the protective iron sulfide layer exposing bare steel to further sulfidic attack and higher rates of corrosion [26].

Liu, Dean and Bosen investigated the corrosion rate of carbon steel, inside methyldiethanolamine solution, versus room temperature, pH, the HSAS concentration and the H_2S loading (mol H_2S/mol amine). The corrosion rate of the steel increased when the ratio of the H_2S reduced. According to their report at 0 to 0.002 mole H_2S/mole amine loading corrosion rates for both are from 381-406 μm/year, 0.01 mole H_2S/mole amine loading corrosion rates are reduced to 127-152 μm/year and at 0.05 mole H_2S/mole amine loading corrosion rates fall to 51-76 μm/year. This reduction of the corrosion rate implies that on carbon steel is formed a protective film of iron sulfide. However, if the loading is bigger than the 0.35 the corrosion rate increased [27].

2.3 Material

The steel, that used for an amine absorber column, is a C-Mn (Carbon-Manganese) or ferritic steel, which according to ASTM standard A516 [28] is categorized in 4 Grades (55, 60, 65, 70). As the grade grows, the higher it the tensile strength, in contrast to the elongation which is decreasing. The material is normally used in applications requiring moderate to low temperature service where excellent notch toughness is important. A significant quantity of ASTM A516 Grade 60 boiler quality plate is used by pressure vessel manufacturers and fabricators making process equipment for the oil and gas industry. Some is also used for skid mounted pressure vessels and modules on production platforms and much is used in refineries and downstream processes.

To avoid impurities and decrease unexpected failures the material suffered melting practices. Such as vacuum induction melting (VIM) and vacuum arc melting (VAM). Due to the corrosive environment used, the steel was tested by the NACE standard TM-0284.

This standard test method, is to designed to evaluate, specifically to material's resistance to HIC and not the others failures expect the sour environments like as SSC, SWC, blister cracking.

The unstressed specimens, i.e. pipe, they created as specified by the method and exposing to one of the two standard test solutions. Solution A, a sodium chloride, acetic acid (NaCl, CH_3COOH) solution saturated with H_2S at ambient temperature and pressure, or Solution B, a synthetic seawater solution saturated with H_2S at ambient temperature and pressure. After a specified time, the test specimens shall be removed and evaluated the amount of the HIC which was created [29].

2.3.1 Vacuum induction melting (VIM).

According to ASM Handbook, the vacuum induction melting is used to removal of undesired trace elements with high vapor pressures which must kept under very low concentration in metal to avoid unexpected failure. The primary process of this method, is the deoxidation. Deoxidation is calling the following reaction:

$C + O \rightarrow CO$

With this reaction the oxygen remove form the melt. In addition to, this reaction decreased the carbon and produce steels with low carbon. Also, the vacuum melting is used to remove impurities by disassociation, flotation or volatilization, nitrogen and hydrogen gasses, from the steels.

A VIM furnace, as it shown in Figure 5, melts the steel and at the same time is connecting with a vacuum system to avoid blend impurities with the melting alloy. The furnace contains induction coils and cooling coils. Induction coils are flowing by electric and heat the charge material to being molten. These coils except that heating the charge materials, creates magnetics fields that require current in the charge. The cooling coils are used to cool the inductions coils by water flowing through the tubing.

The new furnaces operated under variable frequency and the melt can controlling to obtain the most rapid heating/melting conditions [30].

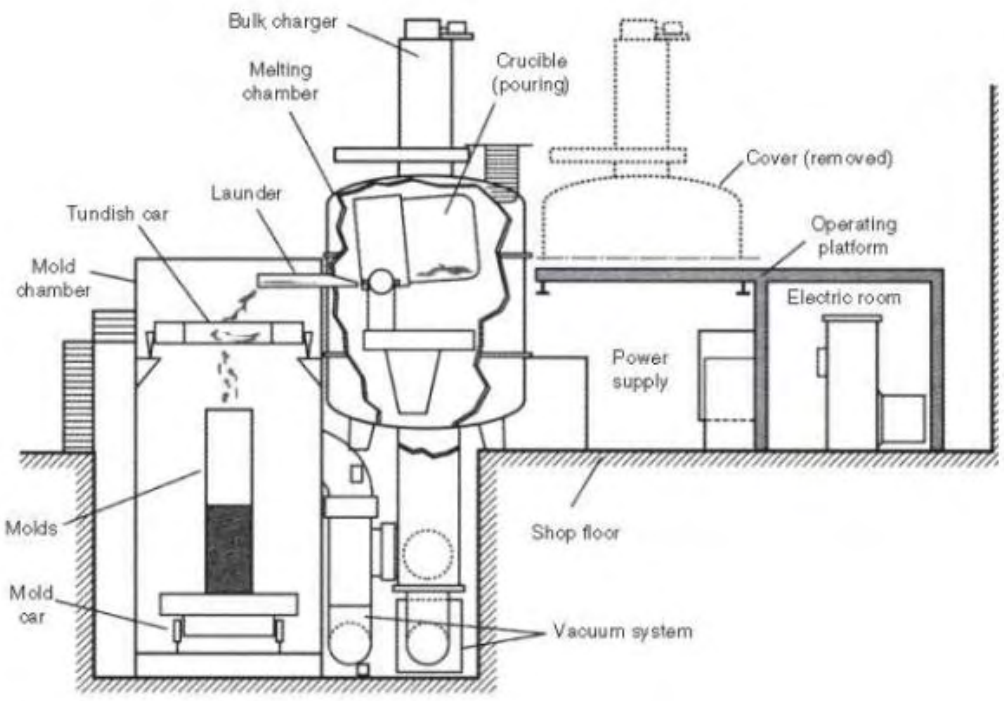

Figure 5. Schematic of a top-opening, double-chamber vacuum induction melting furnace [31].

2.3.2 Vacuum Arc Remelting (VAR).

The vacuum arc remelting is used to improve the cleanliness and refine the structure of standard air-melted or vacuum induction melted ingots. The fields of application are the aerospace, power generation, chemical industry, medical and nuclear industries.

Two major mechanical assemblies combine to form the vacuum vessel in which melting occurs - the movable furnace head and the fixed melt station. The movable furnace head is the upper section of the vessel. An integral ram assembly connected to a highly sophisticated servo drive supports and controls the movement of the electrode. The water-cooled ram extends through a vacuum seal in the head and the electrode clamps to its lower extremity thus becoming the cathode of the arc melting operation. The fixed melt station, which forms the lower half of the vacuum vessel, consists of a removable copper crucible that is placed into a fixed stainless-steel water jacket.

Once the electrode is clamped to the ram assembly the ram lifts the electrode while furnace head is lowered to create a vacuum seal on top of the crucible. Once a vacuum is established, the DC power supply is activated and the control system automatically strikes a high current arc between the consumable electrode (cathode -) and the crucible base (anode +) which quickly forms a molten pool of metal.

The gap between the melting electrode and metal pool (arc gap) is precisely maintained and a controlled melt rate is established. The metal droplets falling through the arc gap are exposed to the vacuum environment and the extreme temperatures of the arc zone. This causes removal of dissolved gasses (such as hydrogen, nitrogen and carbon monoxide), vaporization of undesired trace elements, and improvement in oxide cleanliness, directional solidification of the ingot from bottom to top and removal of inclusions by flotation during remelting. The remaining inclusions are broken up and evenly distributed in the cross-section of the solidified ingot.

Because of the water-cooled crucible, the molten pool of metal formed by the metal droplets is solidified in a directional fashion. When the melt rate and arc gap are correctly controlled this directional solidification prevents macro segregation and reduces the amount of micro segregation thereby enhancing the material properties of the solidified ingot [28, 30, 32].

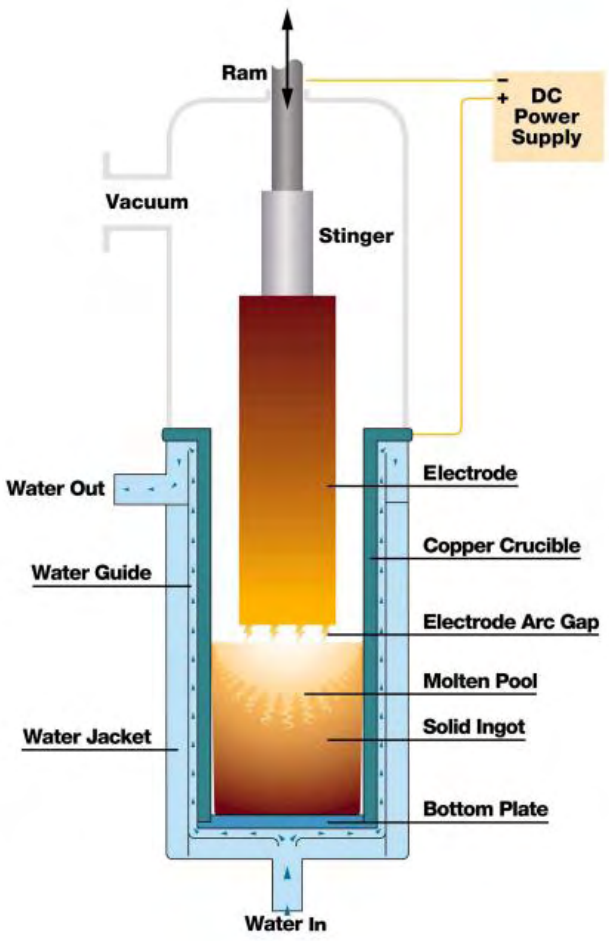

Figure 6. Vacuum Arc Remelting [32].

3 Material Studied

3.1 Amine absorber column

3.1.1 Operating conditions

The column length, without the end cups, is 19 m. The internal diameter is 2.2 m and the shell thickness 91mm. The service is characterized as wet H_2S, H and amine service. The amine was Methyldiethanolamine (MDEA). The operating pressure was 80 Kg/cm^2 and the operating temperature was 70 ^oC. The column had been field-hydrotested before operation. In addition, all the welds had been 100% radiographically inspected while a stress relieving PWHT was performed in all welds. The column operated for 11 years. Following the detection of blistering in the inside diameter (ID), shown in Figure 7, and based on a relevant API level-3 Fitness-For-Service analysis, a decision was made to replace the vessel. In the 6-month period before replacement, hydrogen permeation measurements were conducted at the outside diameter (OD), indicating hydrogen flux values ranging from 10 to 120 pl/cm^{2}s. It is to be noted that hydrogen flux is related to corrosion activity, by H_2S, at the ID. During the 11 years, the vessel operated occasionally at high H_2S/MDEA molar ratio, above the normal ratio of 0.3 reaching values up to 1. It is anticipated that this led to higher corrosion activity and higher hydrogen generation and entry in the material.

3.1.2 Material

The chemical composition, of the studied material, is shown in the Table 1 and the mechanical properties in the Table 2.

Table 1.Chemical Composition

Elements	C	Si	Mn	P	S
Wt. %	0.16	0.2	1.13	<0.01	<0.01

Table 2.Mechanical Properties

Material	SA 516 Grade 60
Tensile Strength (Mpa)	452
Yield Strength (Mpa)	283
Elongation (%)	39

3.2 Experimental Procedures

3.2.1 Sampling Position

A section of absorber column shell cut for investigation. The position of section was 5m from the bottom of the column (Figure 8). In the inside diameter, blistering was evident. (Figure 7)

Figure 7. Blistering in internal surface

The shell section is shown in Figure 8. The section inspected by ultrasonic testing (UT).

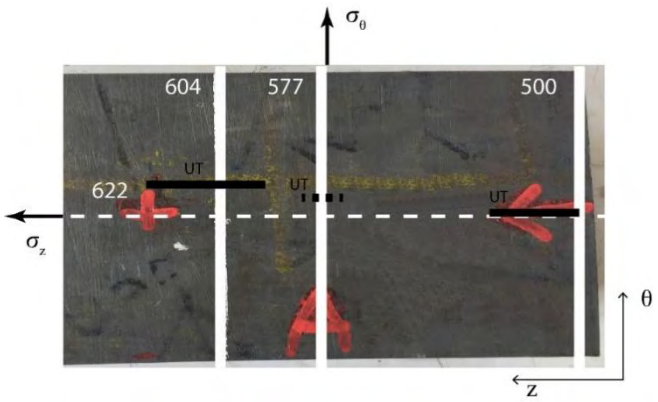

Figure 8. Shell section for analysis

The system of axes used for reference is shown in Figure 9. A cylindrical coordinate system is selected. The axis of the column is the z axis, while the θ axis is the circumferential direction and the r axis is the thickness direction.

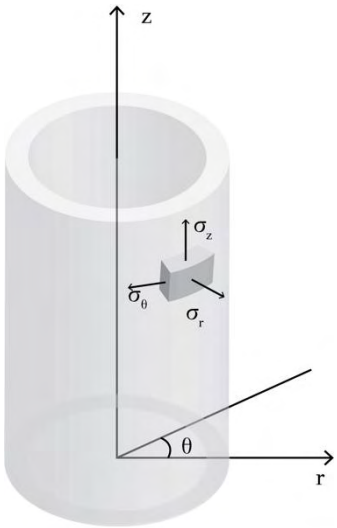

Figure 9. System of axes used for the positioning of specimens.

3.2.2 Ultrasonic Testing.

This technique is used into materials to detect internal flows, characterize them, test the thickness. These materials are steels, metals, alloys and into materials with less resolution like as concrete, wood, composites. Also, it is used in many industries including steel and aluminum construction, metallurgy, manufacturing, aerospace, automotive and other transportation sectors.

In ultrasonic testing, an ultrasound transducer connected to a diagnostic machine is passed over the object being inspected. The transducer is typically separated from the test object by a couplant (such as oil) or by water, as in immersion testing. However, when ultrasonic testing is conducted with an Electromagnetic Acoustic Transducer (EMAT) the use of couplant is not required.

There are two methods of receiving the ultrasound waveform: reflection and attenuation. In reflection (or pulse-echo) mode, the transducer performs both the sending and the receiving of the pulsed waves as the "sound" is reflected back to the device. Reflected ultrasound comes from an interface, such as the back wall of the object or from an imperfection within the object. The diagnostic machine displays these results in the form of a signal with an amplitude representing the intensity of the reflection and the distance, representing the arrival time of the reflection. In attenuation (or through-transmission) mode, a transmitter sends ultrasound through one surface, and a separate receiver detects the amount that has reached it on another surface after traveling through the medium. Imperfections or other conditions in the space between the transmitter and receiver reduce the amount of sound transmitted, thus revealing their presence. Using the couplant increases the

efficiency of the process by reducing the losses in the ultrasonic wave energy due to separation between the surfaces.

Locations with UT signals are indicated by thick black horizontal lines (UT) in Figure 8. The positions of the metallographic sections are indicated by perpendicular white lines. Three positions were considered in this work: positions 500, 577, and 604, which pass through the UT signals. The numbers indicate distances, in mm, from a reference point on the vessel shell. It should be noted that the UT signal from position 577 was scattered and not concentrated in a line, as the signals from positions 500 and 604. As will be shown below, the UT signals from positions 500 and 604 correspond to SOHIC cracking, while the signal from position 577 corresponds to HIC, i.e., isolated HIC cracks without linking. An explanation is provided in Figure 10, correlating the UT signal with the respective metallographic section.

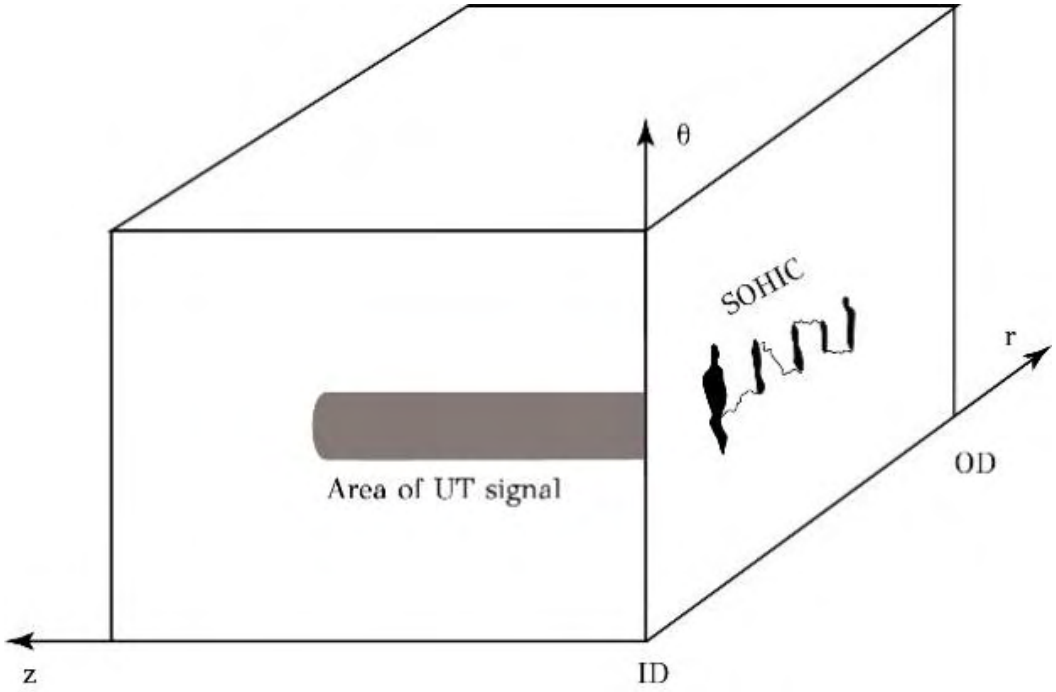

Figure 10.Positions of UT signals

3.2.3 Metallographic

All specimens, from the above sampling position, were prepared using classical metallographic techniques. The specimens were cut from the plate of the corresponding material with the use of a cutting machine (Struers Discotom).

The specimens were initially grinded on SiC abrasive wheels. The sizes of grains were 120, 220, 320, 500, 800, 1000 grid. Polishing of the specimens followed on special disks with diamond paste of 3μm and 1μm grain size respectively.

The surface was chemically etched with 4% Nital reagent. Nital is a solution of nitric acid and alcohol. This reagent has a chemical composition of: 96ml C_2H_5OH and 4 ml HNO_3[33]. The specimens were washed with distilled water and alcohol and dried in a purge of warm air.

Finally, the specimens examined by optical metallographic microscope, Leitz "Aristomet" (Leica Camera AG, Germany) at magnification 50x–500x.

3.3 Mechanical Testing

3.3.1 Tensile Test

A tensile test is used to identification the material properties. These are Young's Modulus, Elastic Modulus, Tensile Modulus, Yield Strength (or Yield Point) and Offset Yield Point or Proof Stress. This test forms a diagram of Stress (or applied force) function to Strain (or change in length) (Figure 11) though the machine's program. The information for the diagram is carried out from the force which apply the machine's grabs onto the specimen and also, from an elongation meter which is placed above the specimen [34].

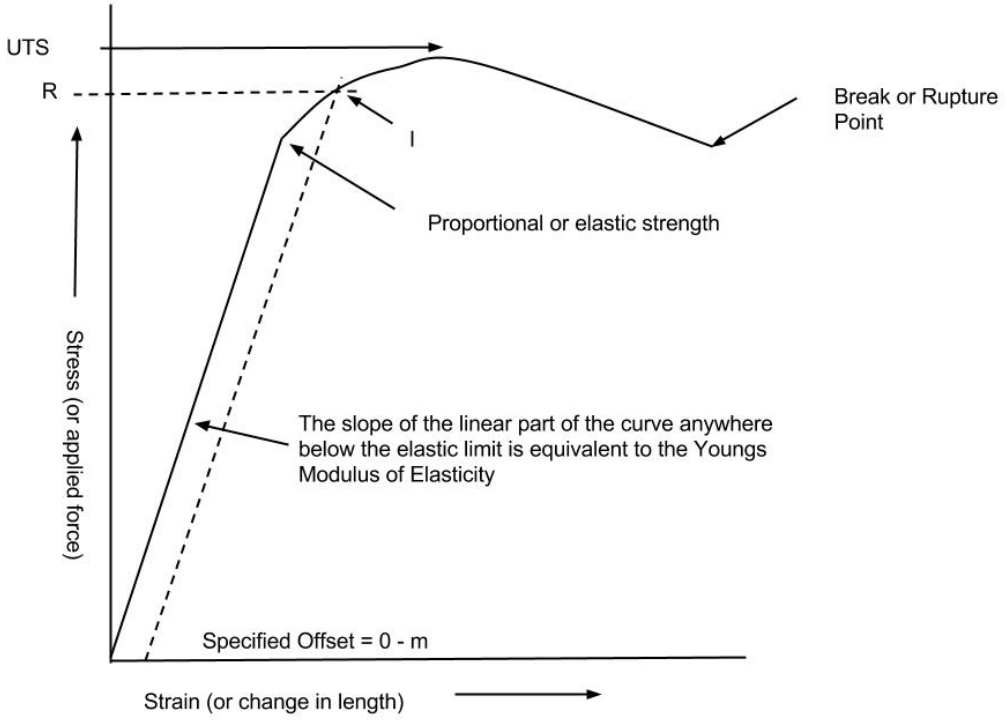

Figure 11. Diagram of Tensile Test

The standard that used is ASTM EN10002-1:2001 and the test are occurred in destructive testing lab at university of Thessaly. This standard covers the tensile testing of metallic materials. Method of this test as elevated temperatures. The specimens for this and rest tests extracted form a region with no UT signals, i.e., a region free from cracking (HIC or SOHIC). The exact locations of the tensile specimens relative to the inside diameter (ID) and outside diameter (OD) are shown in Figure 12 of the paper.

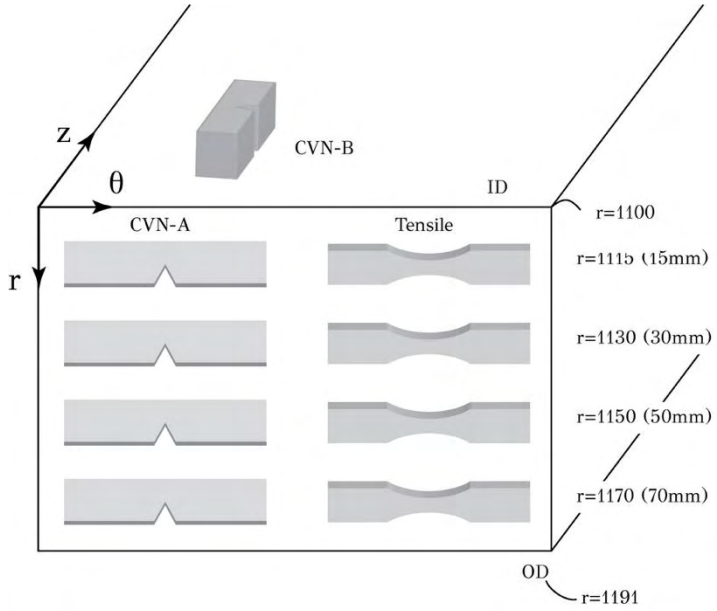

Figure 12.Positions of tensile specimens as well as CVN-A and CVN-B specimens relative to ID and OD.

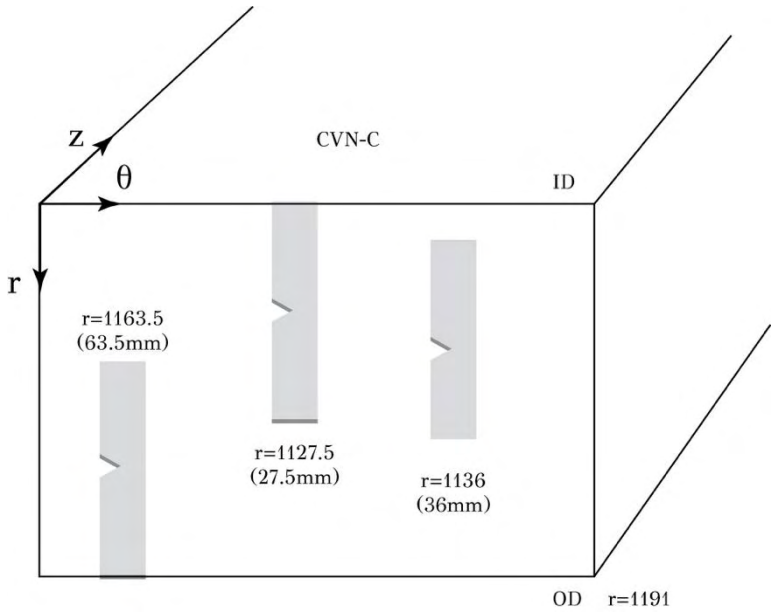

Figure 13.Positions of the CVN-C specimens relative to ID and OD.

3.3.2 Charpy–V–Notch

The most common Charpy's impact test method is the V–Notch Charpy and method Izod. In this project the method that used is V–Notch Charpy. The impact test is a destructive testing, like the tensile test, which is used to identification the relationship of ductile to brittle transition in absorbed energy at a series of temperatures. High impact energy corresponds to ductile fracture and low impact energy corresponds to brittle fracture.

The test is performed using several machined bar specimens 1cm x 1cm x 5.5cm with a 2mm deep notch at the middle of a specified flat surface – usually a “V” notch. The specimens are tested at a series of specified temperatures (e.g. -20^{o}C, -10^{o}C, 0^{o}C, +10^{o}C, +20^{o}C). Once a specimen reaches the precise temperature, it is quickly placed into a special holder with the notch oriented vertically and toward the origin of impact. The specimen is struck by a “tup” attached to a swinging pendulum of specific design and weight. The specimen breaks at its notched cross-section upon impact, and the upward swing of the pendulum is used to determine the amount of energy absorbed (notch toughness) in the process [34].

Tests are occurred in destructive testing lab at Ebetam S.A and the standard that used in this project was ASTM E23. For the CVN testing, three specimen orientations were used, depicted in Figure 12Figure 13. In the CVN-A configuration, the specimen length is along the transverse direction (q) and the notch is in the thickness (r) direction. In the CVN-B configuration, the specimen length is along the longitudinal axis (z) of the vessel shell and the notch in the transverse (q) direction. In the CVN-C configuration, the specimen length is along the thickness direction of the shell (r) and the notch in the transverse direction (q). Two impact test specimens were tested for each location.

3.3.3 Vickers hardness test (HV), 0.3 kg

Hardness is a measure of the resistance to localized plastic deformation induced by either mechanical indentation or abrasion. The square-base pyramidal diamond indenter is forced under a predetermined load ranging from 1 to 120 kg into the material to be tested. After the forces have reached a static or equilibrium condition and further penetration ceases, the force remains applied for a specific time (10 to 15 s for normal test times) and is then removed. The resulting unrecovered indentation diagonals are measured and averaged to give a value in millimeters. These length measurements are used to calculated the Vickers hardness number (HV). The Vickers hardness number (formerly known as DPH for diamond pyramid hardness) is a number related to the applied force and the surface area of the measured unrecovered indentation produced by a square-base pyramidal diamond indenter. The Vickers indenter has included face angles of 136° and the Vickers hardness number (HV) is computer from the following equation:

$$\mathrm{HV}=\frac{2P}{d^2}\sin\frac{136^o}{2}$$

where P is the indentation load in kg, and d is the mean diagonal of indentation, in mm [34].

3.3.4 Fractography

Fractography is used to determine the cause of failure in engineering structures. With this method it is impossible to develop and evaluate theoretical models about the grown of the failure.

The crack growth is shows up in different type. For example, fatigue, stress corrosion cracking, hydrogen induced cracking or stress orient hydrogen induced cracking have got different growth behavior.

Common features that may cause crack initiation are inclusions, voids or empty holes in the material, contamination, and stress concentrations. "Hachures", are the lines on fracture surfaces which show crack direction. The broken crankshaft shown at right failed from a surface defect near the bulb at lower center, the single brittle crack growing up into the bulk material by small steps, a problem known as fatigue. The crankshaft also shows hachures which point back to the origin of the fracture. Some modes of crack growth can leave characteristic marks on the surface that identify the mode of crack growth and origin on a macro scale e.g. beach marks or striations on fatigue cracks. The areas of the product can also be very revealing, especially if there are traces of sub-critical cracks, or cracks which have not grown to completion. They can indicate that the material was faulty when loaded, or alternatively, that the sample was overloaded at the time of failure [35].

The crack at location 604 was opened for fractographic analysis by Dr. Kyriaki Polychronopoulou in the laboratory of the department of mechanical in the Khalifa university of Science and Technology. In order to open the crack, a section containing the crack was cut and cooled to -30 ^{O}C for 24 h. Then, the section containing the crack was put in an anvil. The crack was opened by impact on one side of the section with a hammer. A small section of “fresh” fracture area was generated. Investigation of the fracture surface was performed in a JEOL JSM-7610F SEM (JEOL, Tokyo, Japan) equipped with a field emission gun. The operating voltage was 20 kV.

4 Results and Discussion

4.1 Material characterization

The tensile properties are shown in Table 3. In addition to yield strength, ultimate tensile strength, and elongation, the elastic modulus was determined to be 210 GPa. In general, the measured properties agree with the manufacturer's data. Although there is a slight decrease in the ultimate tensile strength relative to the manufacturer's data, the elongation of the material is high and indicates a ductile material. This argument is also in agreement with the impact test results, which are shown in Table 4Table 5Table 6 for CVN-A, CVN-B, and CVN-C configurations respectively. All notch configurations exhibited high impact values that do not indicate any deterioration of the notch ductility of the material in the regions away from cracking. In other words, the observed cracking was highly localized. Finally, the Table 7 contain the result of Hardness Test Vickers.

Table 3.Tensile test results at different locations throughout the thickness of the plate.

Location (mm from ID)	Yield Strength (MPa)	UTS (MPa)	Elongation (%)
15	290	432	46.4/45.06
30	287	430	42.26/37.2
50	291	439	38.0/39.4
70	286	438	40.4/38.5
Manufacture Data	283-285	445-452	38-39

Table 4. Results from CVN-A impact test configuration.

Notch Position (mm from ID)	Specimen ID	CVN Energy (Joule)	CVN Average (Joule)
15	A1/A5	186/194	190
30	A2/A6	184/180	182
50	A3/A7	170/186	178
70	A4/A8	168/168	168

Table 5. Results from CVN-B impact test configuration.

Notch Position (mm from ID)	Specimen ID	CVN Energy (Joule)	CVN Average (Joule)
15	B1/B5	186/178	182
30	B2/B6	216/188	202
50	B3/B7	190/192	191
70	B4/B8	184/182	181

Table 6. Results from CVN-C impact test configuration.

Notch Position (mm from ID)	Specimen ID	CVN Energy (Joule)	CVN Average (Joule)
27.5	C3/C6	170/186	178
36	C2/C5	154/160	156
63.5	C1/C4	186/190	188

Table 7. Results from Hardness Test Vickers.

Spec.	1	2	3	4	5	6	7	8	9	10	11
Hv)	147.8	145.7	155.9	143.3	147.7	147.4	136.9	143.7	148.7	137.3	147.7

4.2 Stereoscope

All the specimens are observed by stereoscope. At location 604 are founded HIC and blisters and some of them are connected, Figure 14.

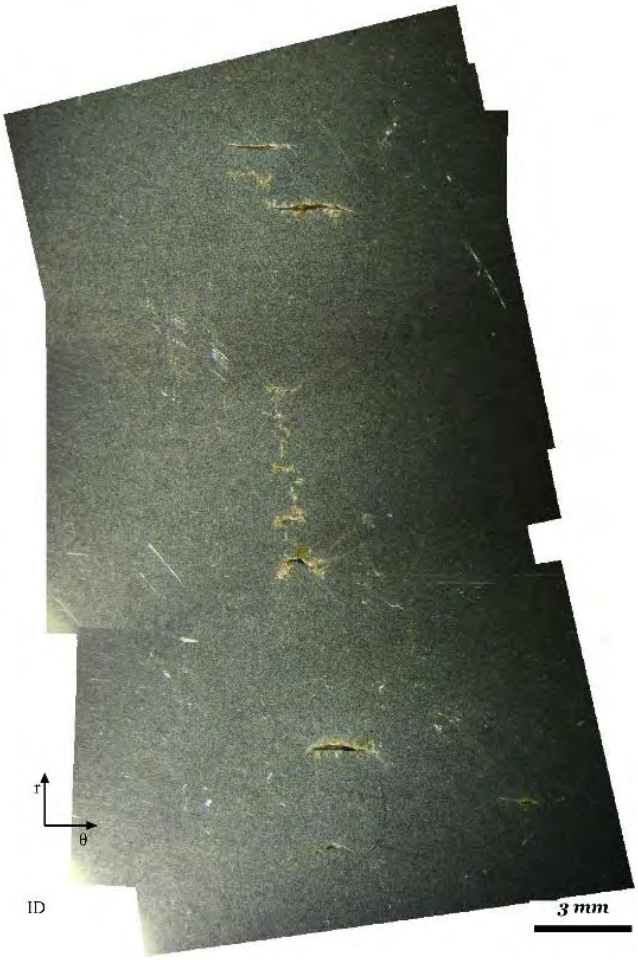

Figure 14. HIC and SOHIC at location 604

The opposing face from the section 500 is observed by stereoscope and in the Figure 15 is shown clearly the hic and a black line which probably is look like sohic.

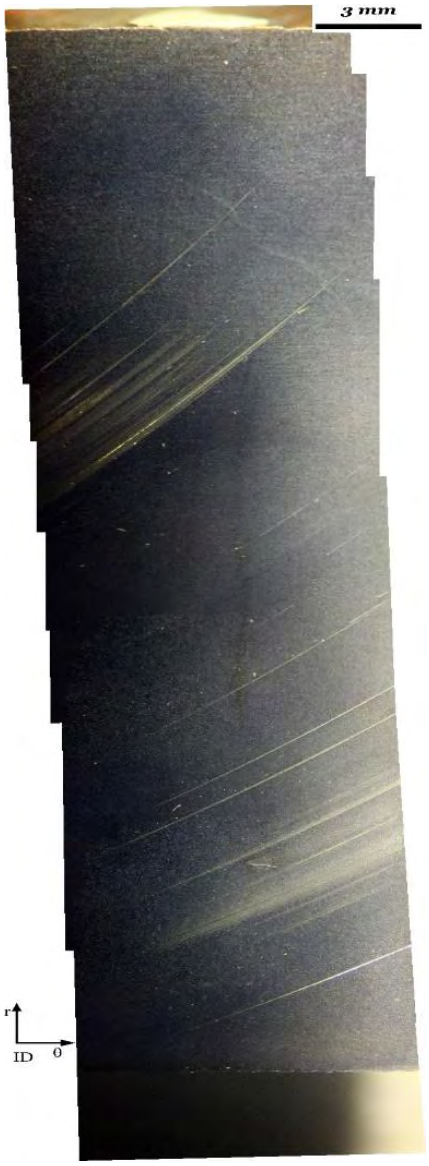

Figure 15. Opposing face at location 500.

At location 577 are observed HIC/blisters near the ID.

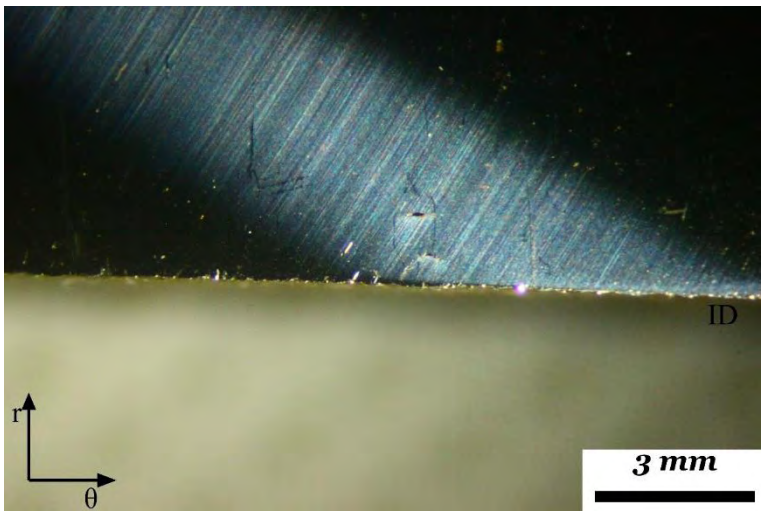

Figure 16. HIC/Blisters at location 577

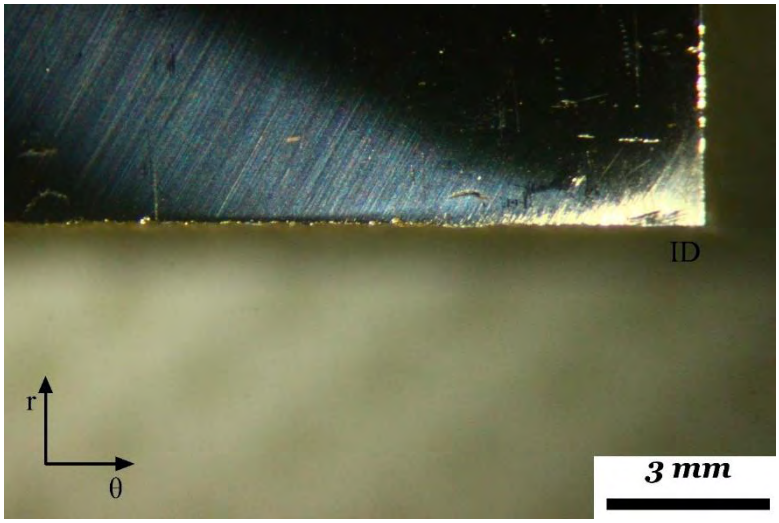

Figure 17. HIC/Blisters at location 577

4.3 Metallographic Characterization of SOHIC and HIC

The microstructure of the steel is depicted in the micrograph of Figure 18, indicating that the microstructure consists of ferrite and pearlite. The white section of the Figure 18 is the ferrite and the black section is the pearlite.

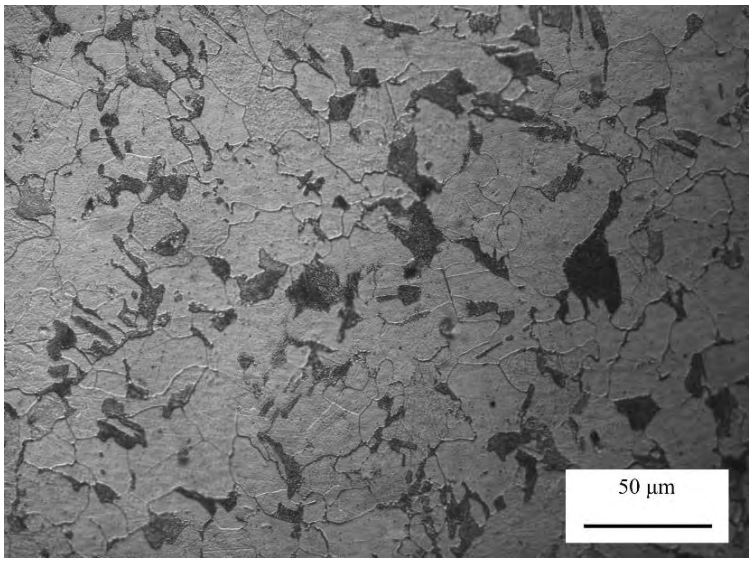

Figure 18. Ferrite-pearlite microstructure of the investigated steel.

The metallographic section at location 604 is shown in Figure 19, which is an assembly of micrographs starting from the inside diameter (ID) of the sell. This is a typical form of stress-oriented hydrogen-induced cracking (SOHIC). Although, microscopically, the crack direction changes several times during propagation, macroscopically, it is a through-thickness crack with a direction perpendicular to the applied stress. The crack appears to interconnect blisters/HIC cracks, which have formed at various levels across the thickness of the plate. The HIC cracks lie on the rolling plane and are stacked normal to the rolling plane. The HIC cracks are linked with cracks which run in a direction normal to the rolling plane and perpendicular to the applied hoop stress. The initiation is at 5 mm from the ID, while the overall crack length is 23 mm.

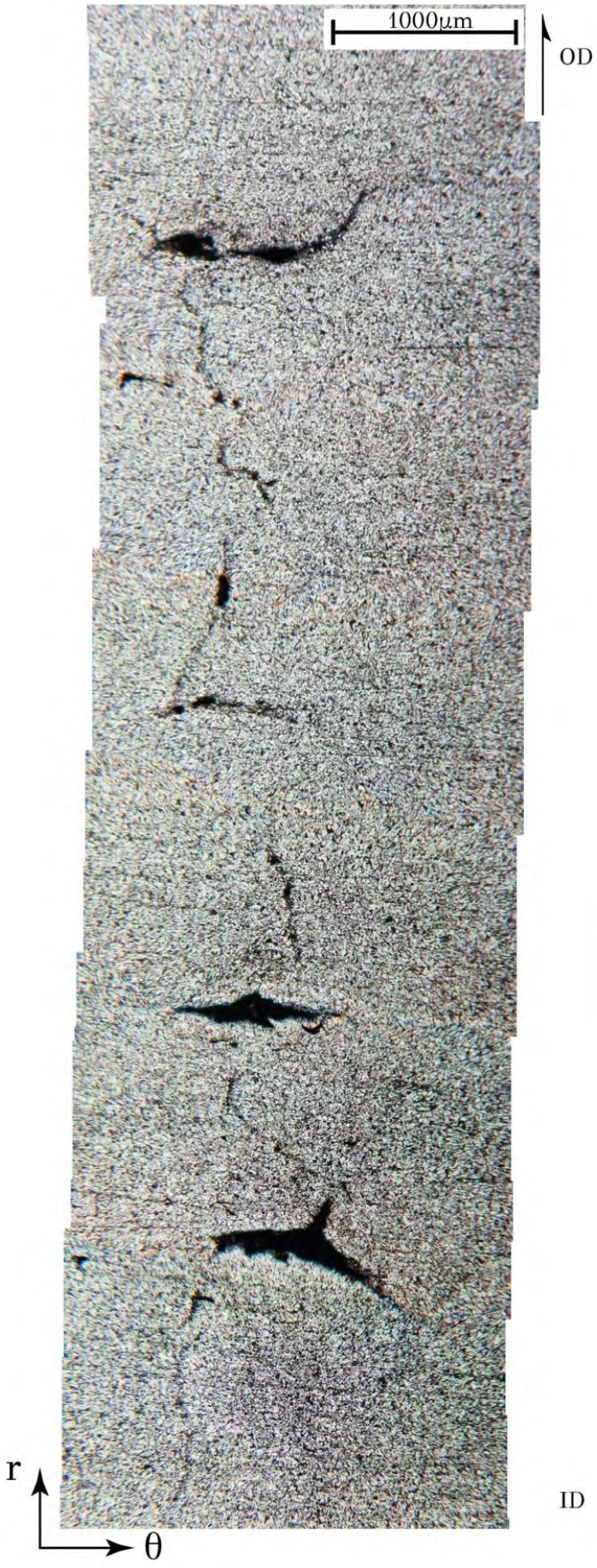

Figure 19. SOHIC at location 604.

There are also some HIC cracks that most of them are founded above and under from SOHIC which probably they are connected with SOHIC, and one of them is founded right from SOHIC.

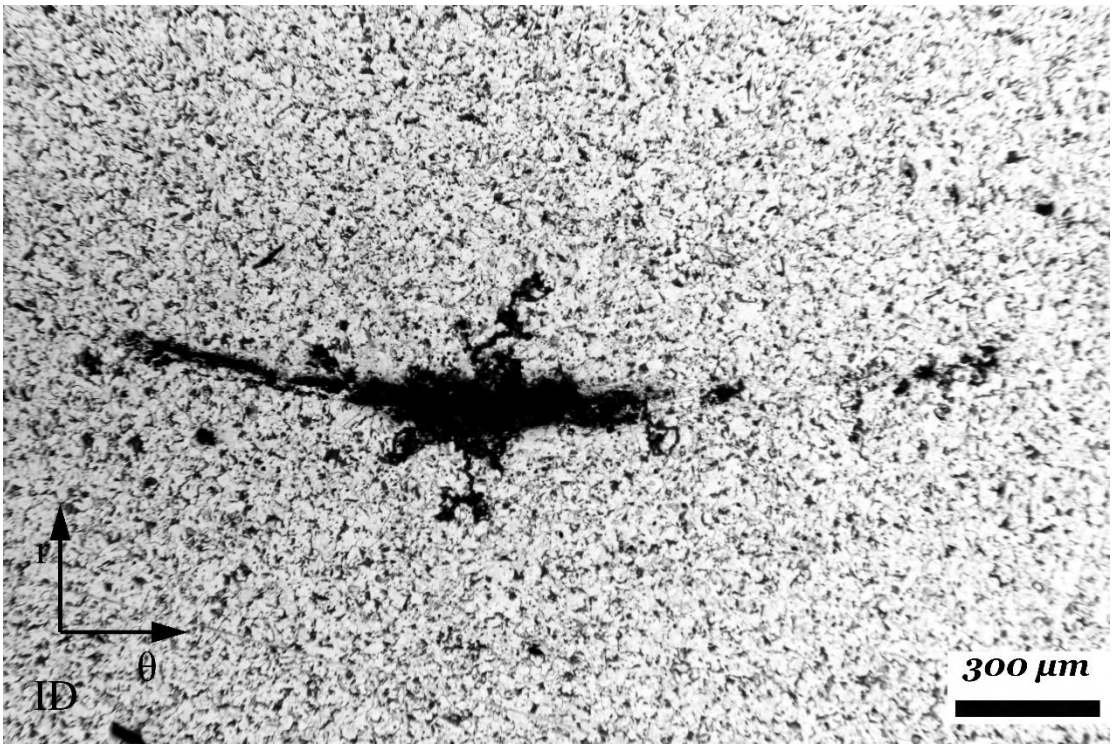

Figure 20. HIC at the location 604, at 1.06mm from ID.

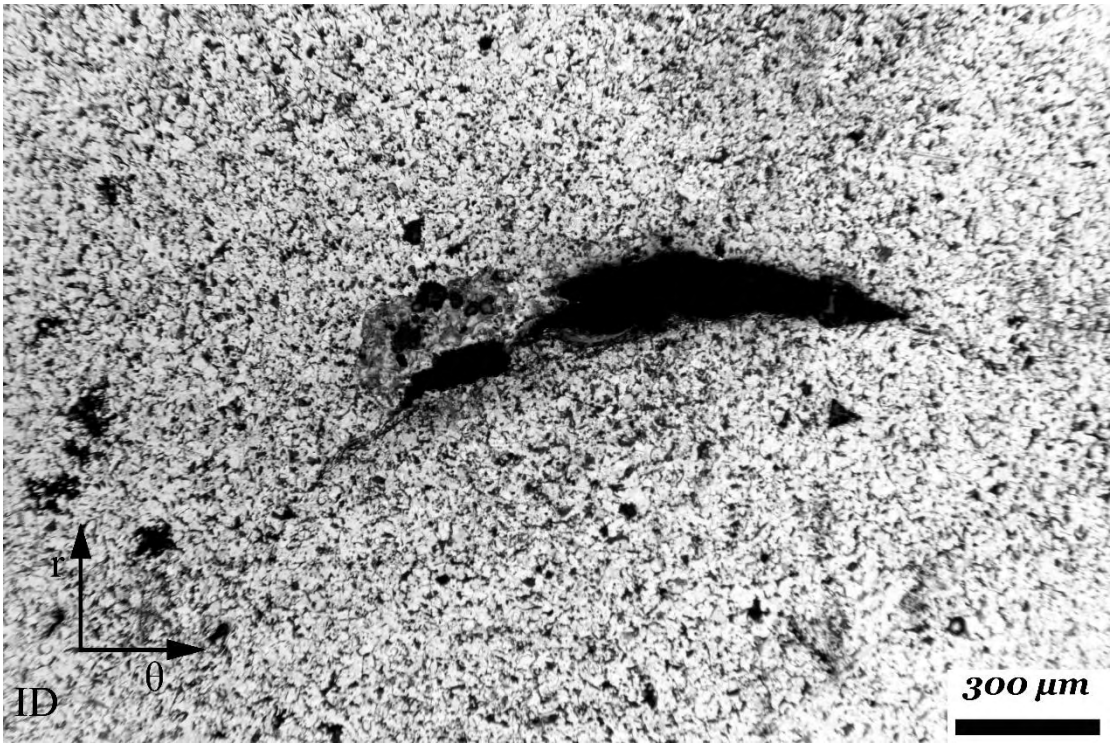

Figure 21.HIC at location 604, at 12.4mm from ID.

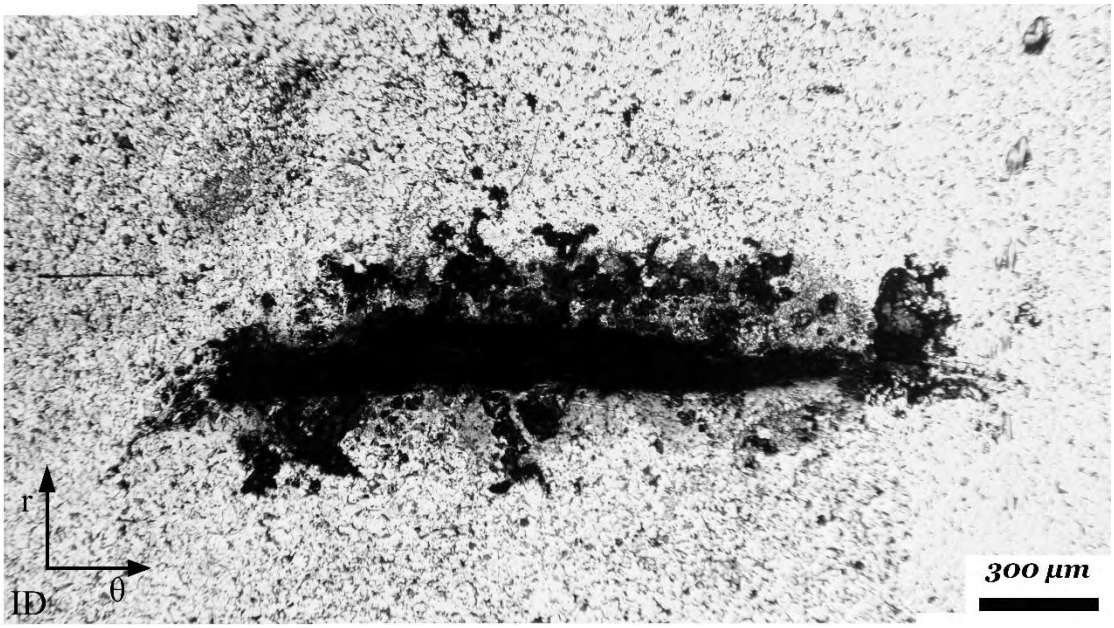

Figure 22. HIC at location 604, at 9.3mm from ID.

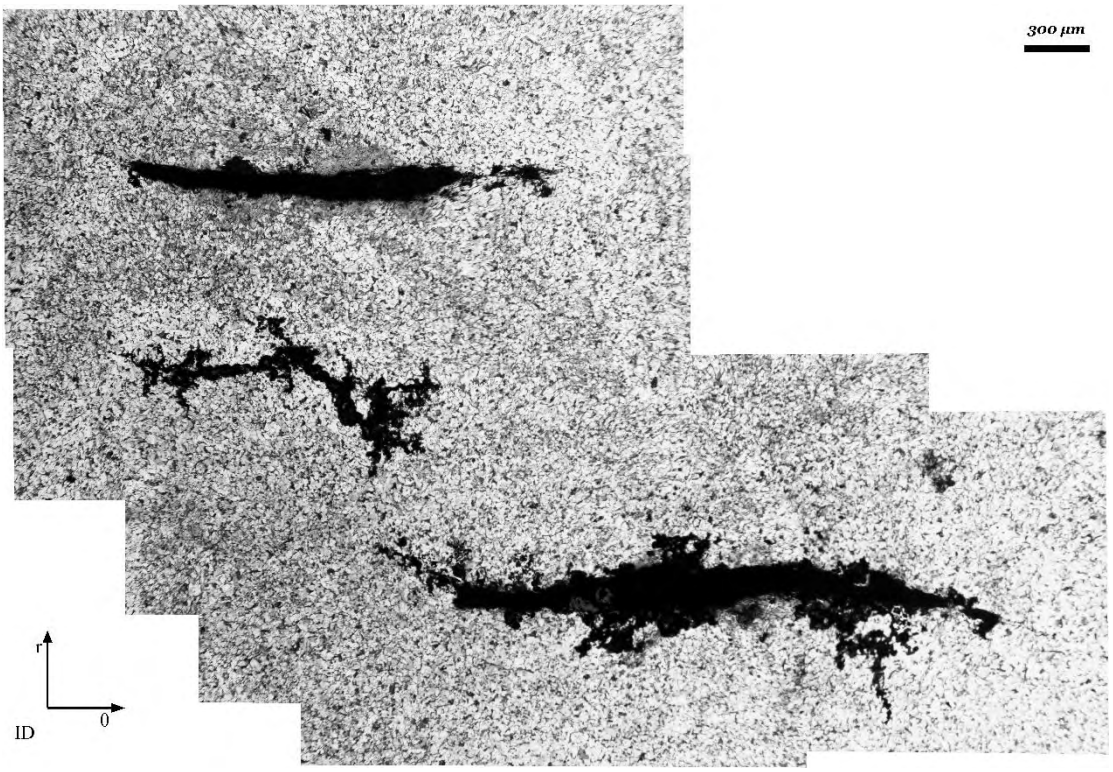

Figure 23. HIC at location 604, at 30.5 from ID.

In Figure 24 is depicted mapping of this section.

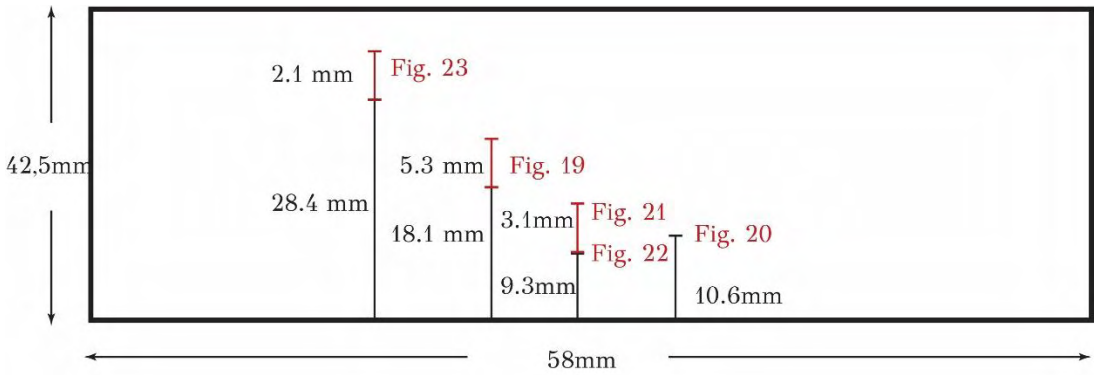

Figure 24. Mapping of section 604

The metallographic section at location 577 is depicted in Figure 25Figure 26,Figure 27. So many blisters/HIC cracks have formed, but they are not interconnected, at least at the plane of observation. This can explain the scattered mode of the UT signal at position 577. The propagation of HIC cracks is through the ferrite phase, between the pearlite colonies at ferrite/pearlite interfaces, as depicted in Figure 28. A similar crack propagation mechanism has been also observed by Gingel and Garat in an API 5L grade X60 pipeline steel [36].

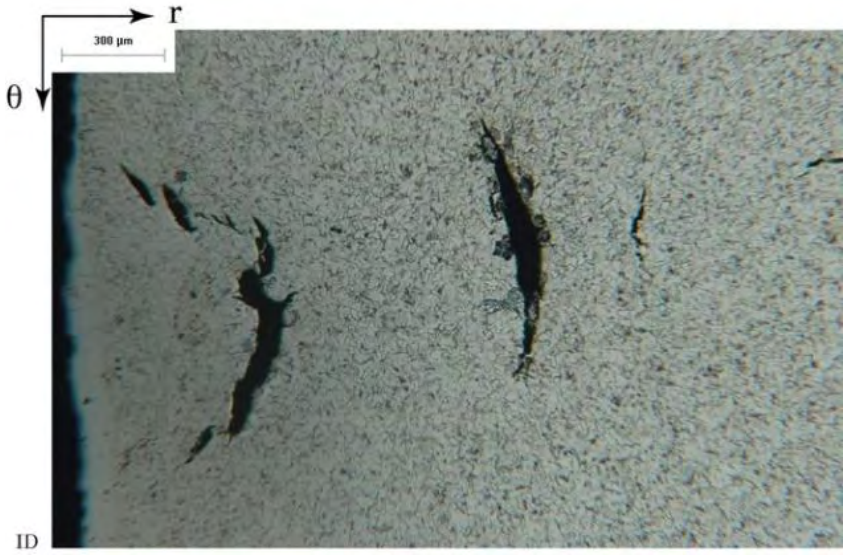

Figure 25.HIC at location 577

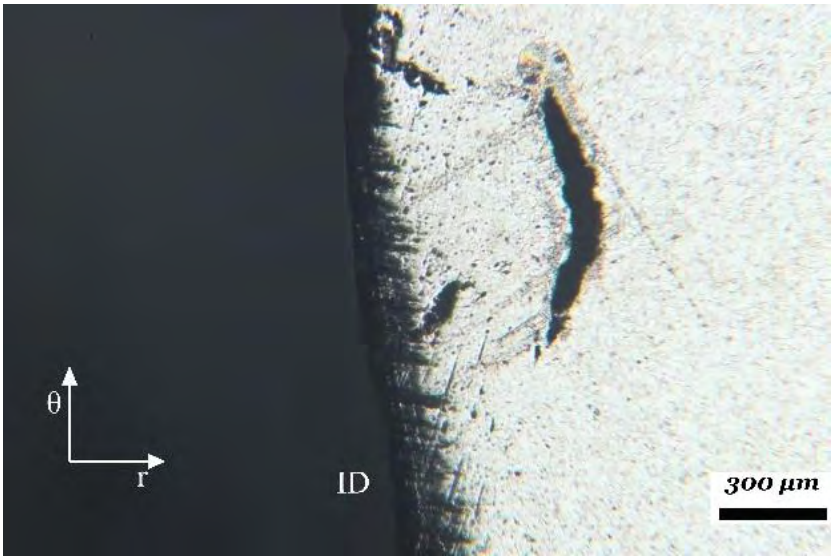

Figure 26.HIC at location 577

Figure 27.HIC at location 577

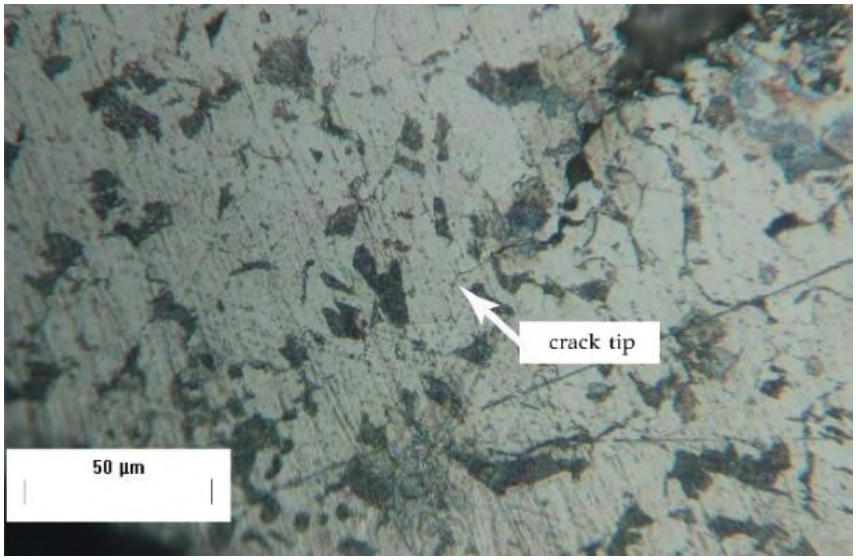

Figure 28. tip of HIC indicating propagation in ferrite between pearlite colonies.

The metallographic section at location 500 is depicted in Figure 29. The crack has initiated at 5 mm from the ID and has an overall length of 30 mm. This type of cracking is also classified as SOHIC.

Figure 29. SOHIC at location 500.

In Figure 30 the metallography of the second corresponding surface, that is revealed after cutting at location 500 is depicted.

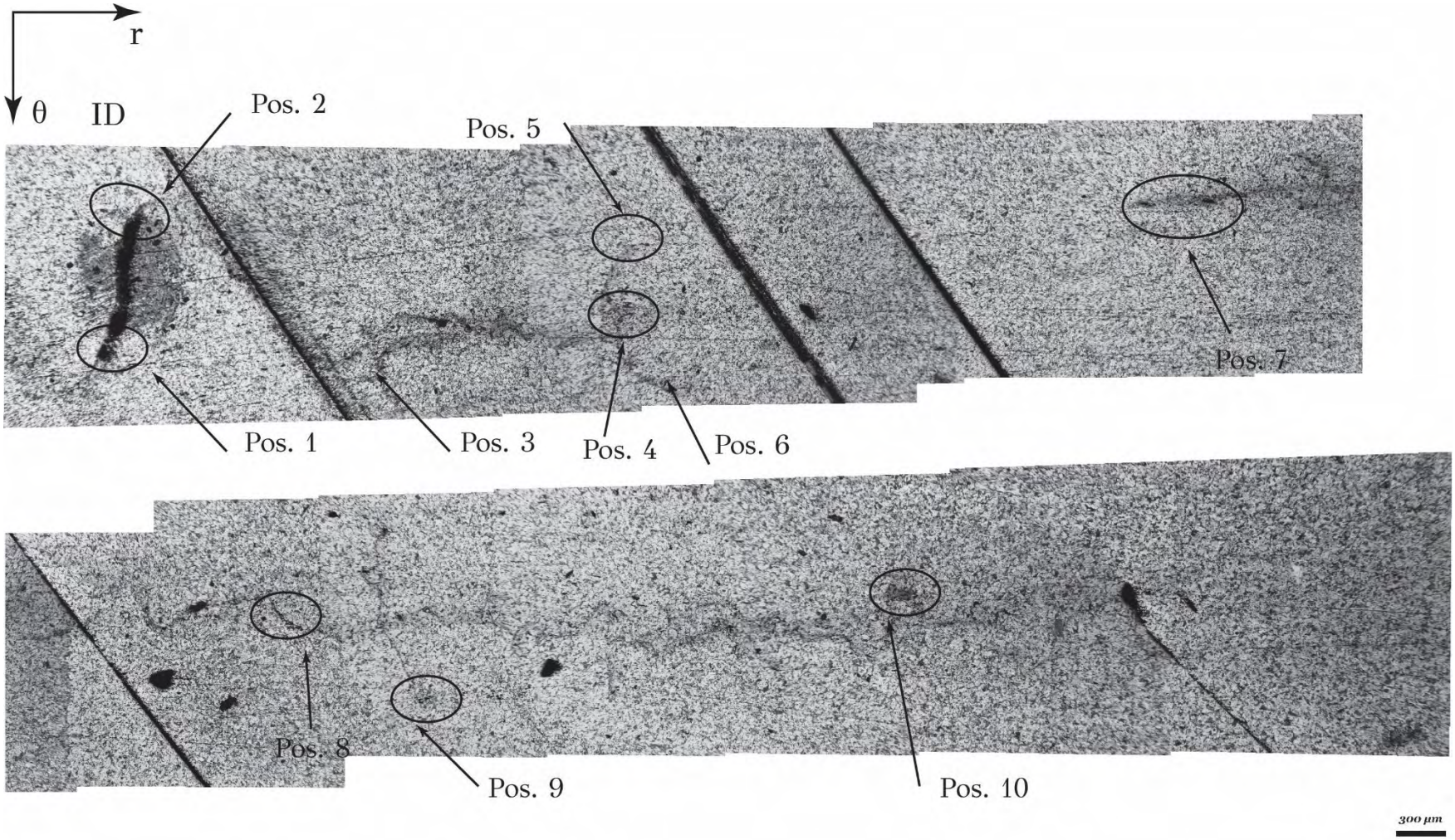

Figure 30. SOHIC at location 500 opposite surface.

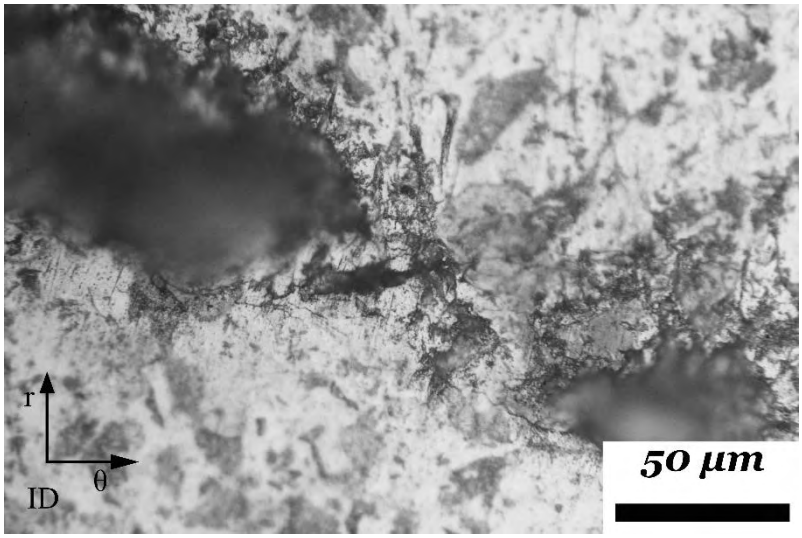

Figure 31. Magnification of ***Error! Reference source not found.*** *in position 1.*

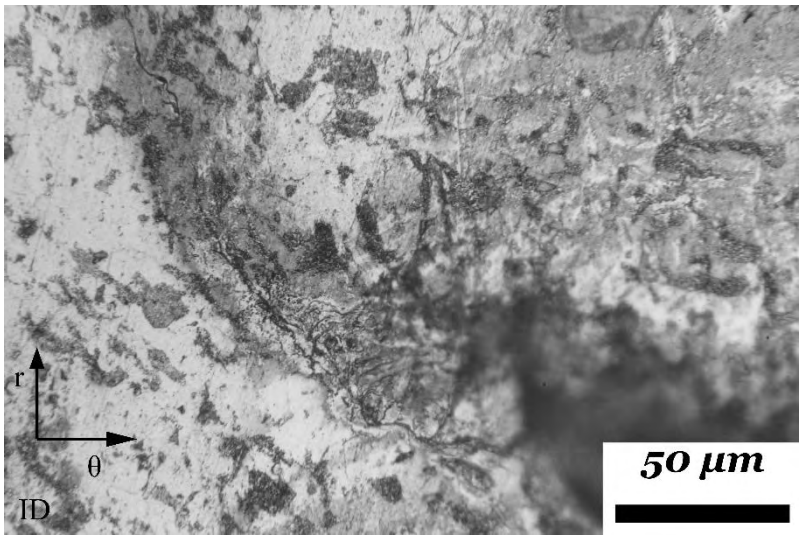

Figure 32. Magnification of ***Error! Reference source not found.*** *in position 2.*

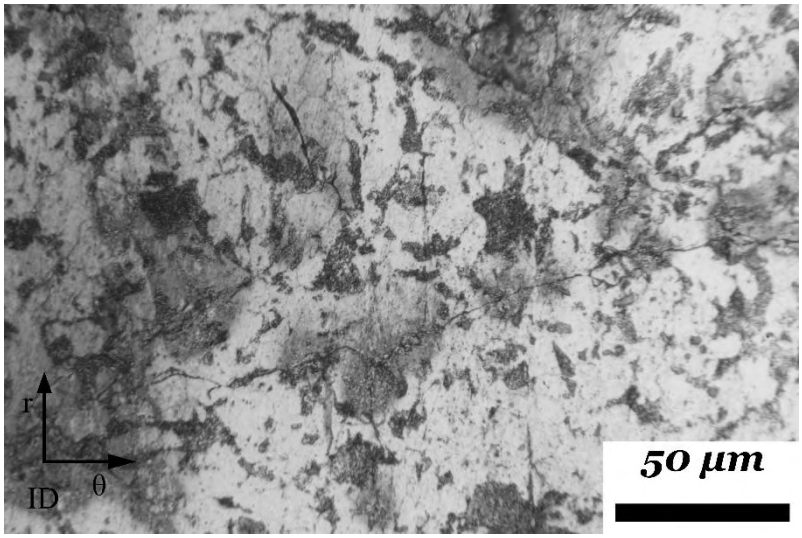

Figure 33. Magnification of ***Error! Reference source not found.*** *in position 3.*

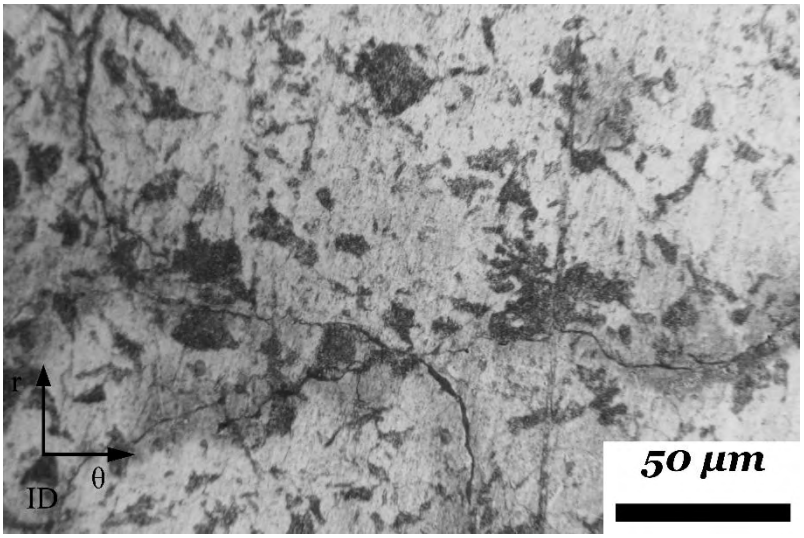

Figure 34. Magnification of ***Error! Reference source not found.*** *in position 4.*

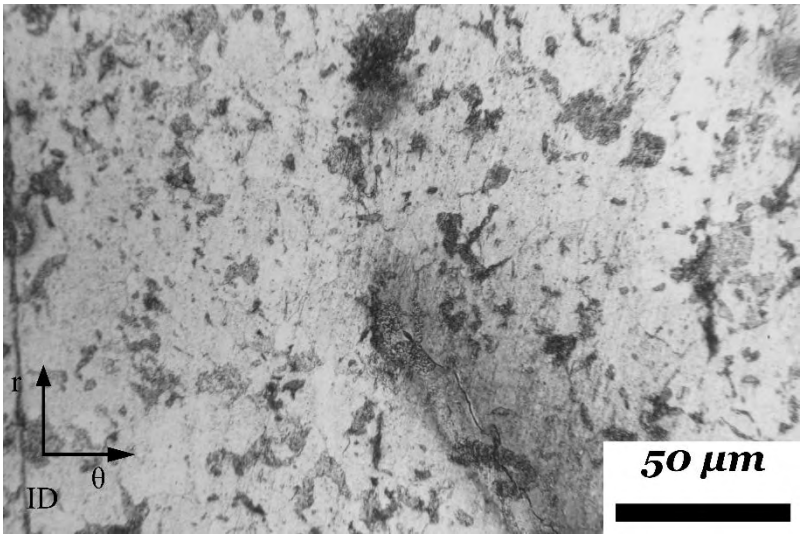

Figure 35. Magnification of ***Error! Reference source not found.*** *in position 5.*

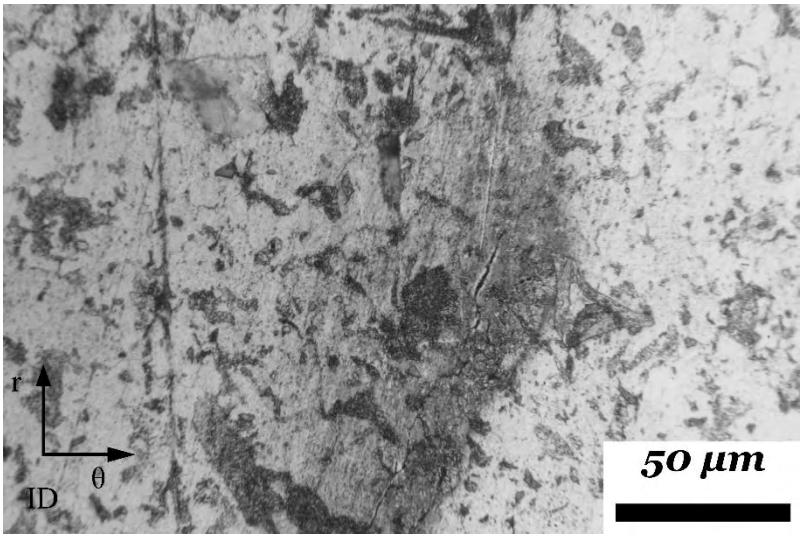

Figure 36. Magnification of ***Error! Reference source not found.*** *in position 6.*

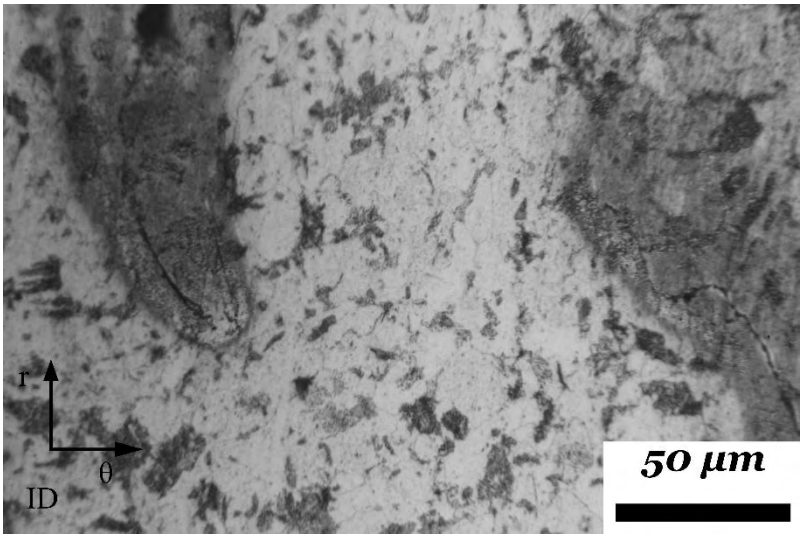

Figure 37. Magnification of ***Error! Reference source not found.*** *in position 7.*

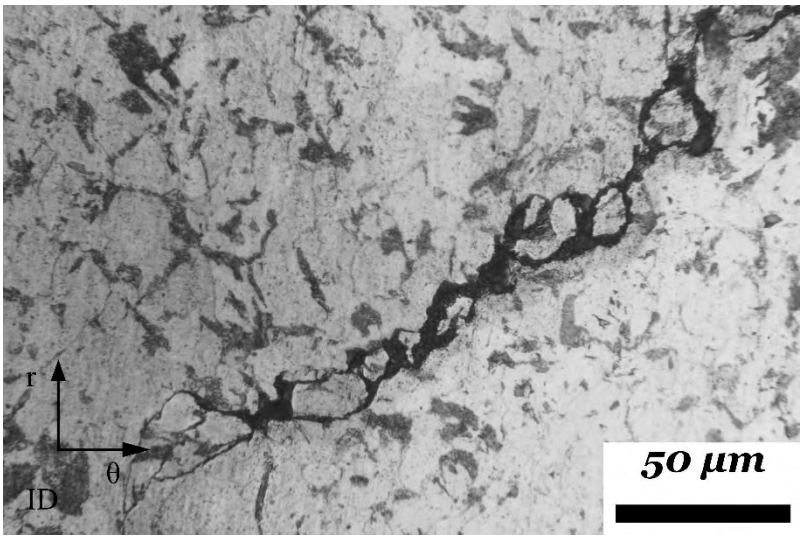

Figure 38. Magnification of ***Error! Reference source not found.*** *in position 8.*

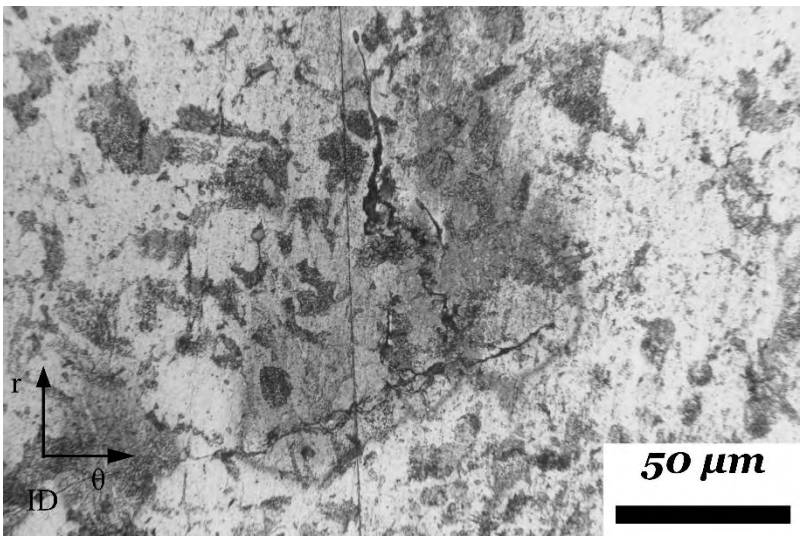

Figure 39. Magnification of ***Error! Reference source not found.*** *in position 9.*

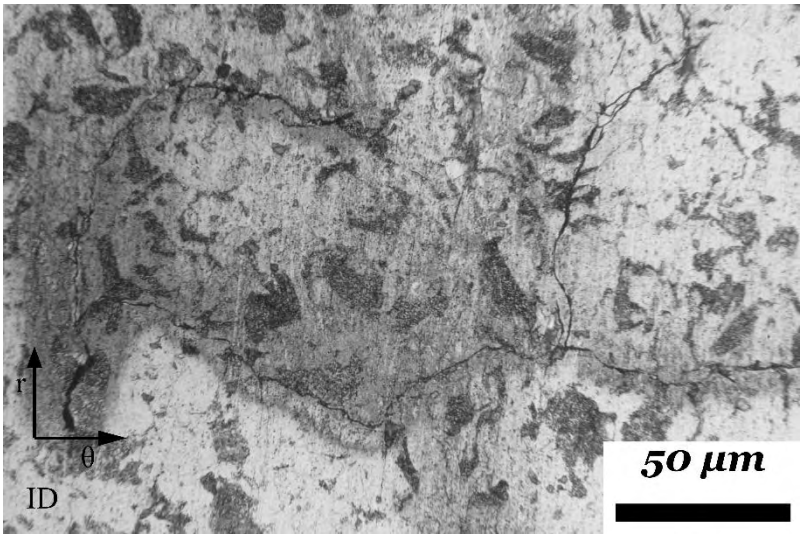

Figure 40. Magnification of ***Error! Reference source not found.*** *in position 10.*

Both cracks at locations 500 and 604 (Figure 19, Figure 29) are, therefore, classified as SOHIC. They interconnect blisters/HIC cracks and they propagate from the ID towards the OD under the action of the applied stress. According to API RP 571 [37], SOHIC consists of arrays of small HIC cracks, initiated at internal blisters in the rolling plane. These HIC cracks are stacked in a direction normal to the applied hoop stress and are linked by cracks normal to the stress. SOHIC should not be confused with stepwise hydrogen-induced cracking (SWC), which exhibits a not-aligned stepped morphology in the absence of stress. The limited cases of SOHIC failures that are reported in Pargeter's review [6] indicate that SOHIC requires a combination of severe hydrogen cracking conditions and stress. In the present case, the amine absorber column was operated under high H_2S/MDEA ratios for certain time periods, promoting high hydrogen charging conditions. In addition, it has been suggested [6] that triaxial loading can encourage the formation of small HIC cracks by increasing the hydrogen solubility in the steel. Stress triaxiality can be induced by the large plate thickness (91 mm). It is expressed by the ratio σ_h/σ, where σ_h is the hydrostatic stress and σ is the von Mises equivalent stress. The triaxiality ratio was calculated (see Appendix A) for the operating conditions and was found as 0.5, which is a number indicating that the material was subjected to a moderate triaxial stress state. In addition, it is interesting to note that the HIC cracks form even though the radial stress is compressive. However, these cracks do not propagate in the rolling plane, but instead they are linked in the radial direction under the action of the hoop stress.

4.4 Fractographic Analysis of Opened SOHIC crack

As discussed above, the SOHIC crack at location 500 was opened for fractographic analysis. A low magnification assembly of SEM micrographs is shown in Figure 41. The region of "fresh" fracture, resulting by the opening procedure and the region of SOHIC fracture are indicated. The boundary between the fresh fracture and SOHIC is depicted in Figure 42. It is clear that there are two fracture modes. The fresh fracture area is

characterized by dimple fracture, also indicated in Figure 43, while the SOHIC area is characterized by cleavage, indicated in Figure 44. In addition, several blisters/HIC cracks can be seen on the fracture surface. The entire SOHIC region, including the areas between blisters is characterized by cleavage as indicated in Figure 45. No black deposit, related to FeS, was found on the fracture surface. In addition, EDX analysis performed on the cleavage areas did not detect the presence of sulfur. The absence of black deposits and sulfur indicate clearly that cracking is not related to sulfide stress cracking (SSC). A large blister/HIC crack is depicted in Figure 46. It was possible to approach the interior of this blister in order to investigate the morphology of the blister wall as it results by the HIC crack opening due to the build-up of hydrogen pressure. The internal wall is depicted in Figure 47, indicating a cleavage fracture surface. Thus, blistering and HIC cracking proceeded with cleavage of the material.

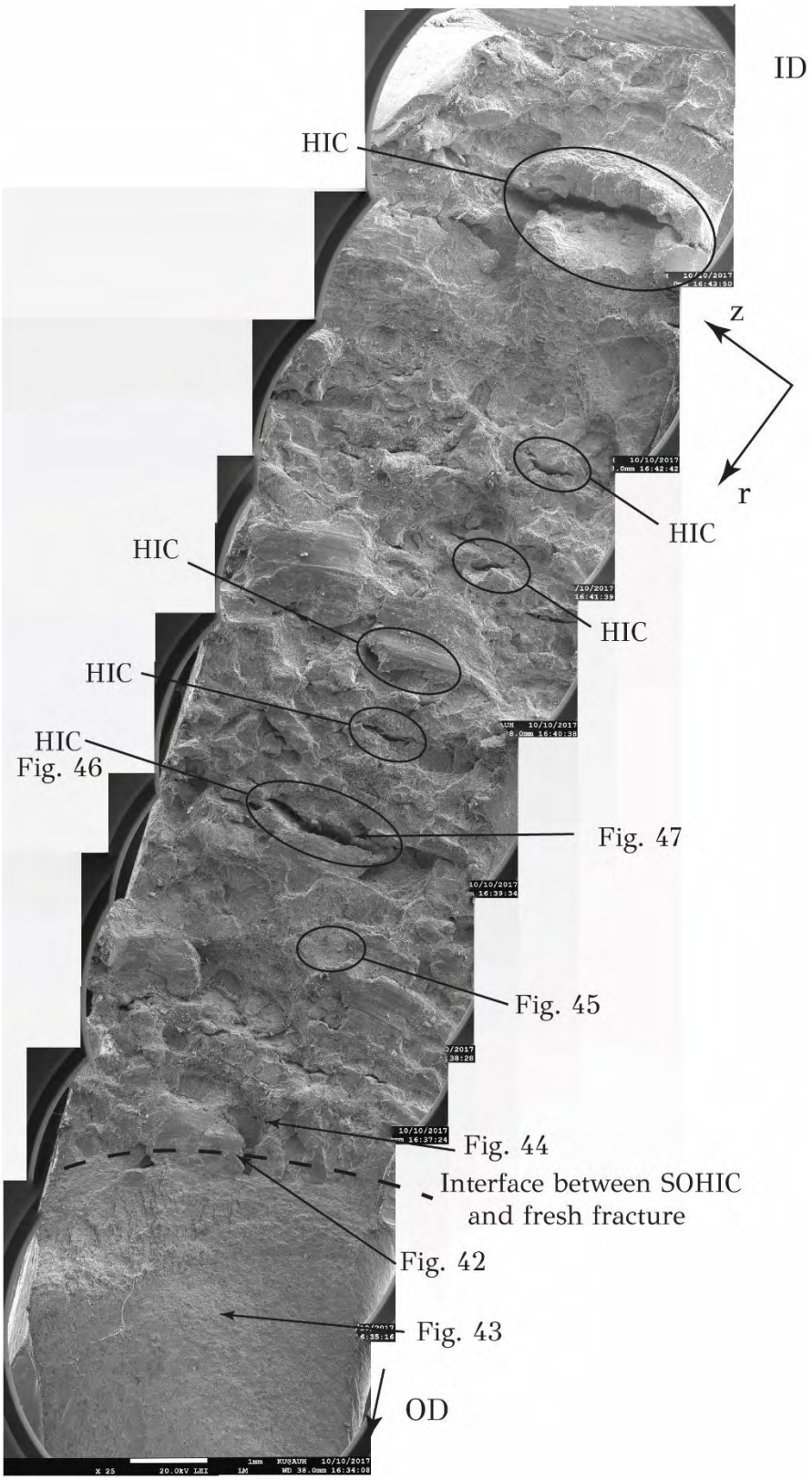

Figure 41. Assembly of SEM micrographs depicting the fracture surface of the opened SOHIC crack at position 500. The location of HIC cracks and individual SEM micrographs is indicated.

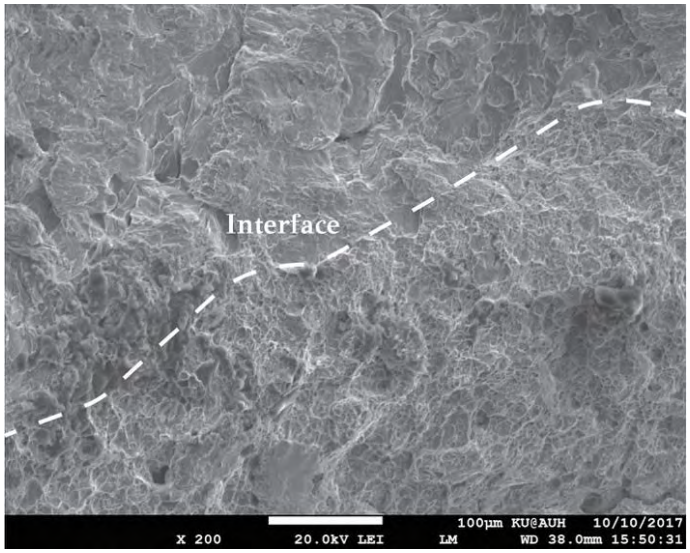

Figure 42. Boundary between SOHIC and "fresh" fracture.

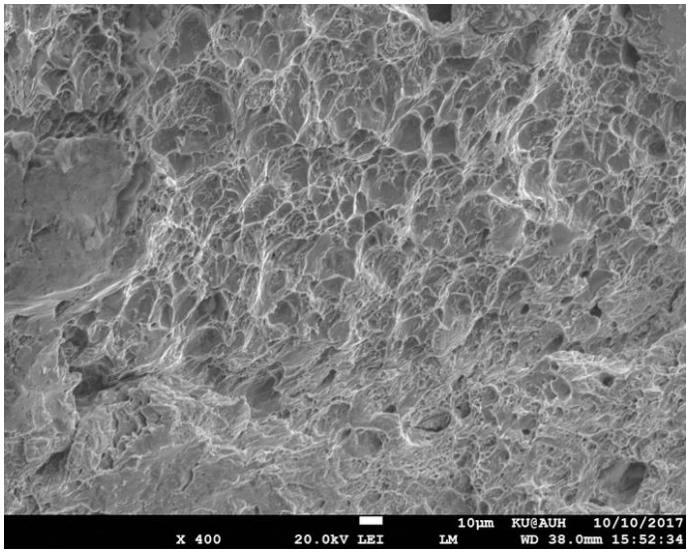

Figure 43.Dimple fracture in the "fresh" fracture region.

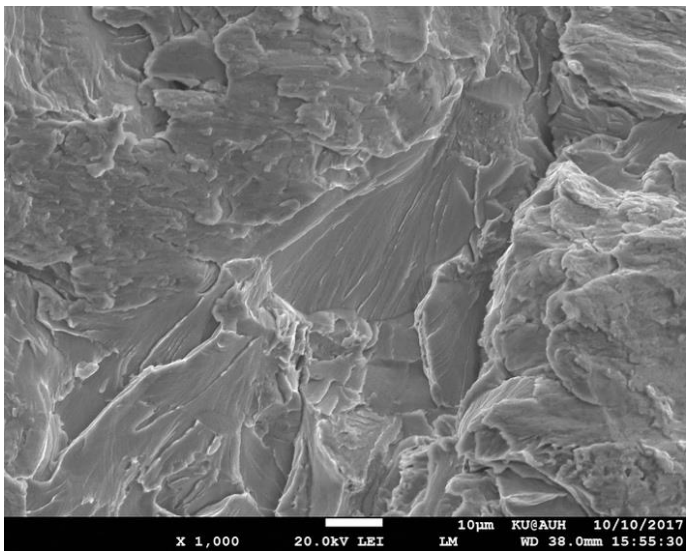

Figure 44. Cleavage fracture at SOHIC region.

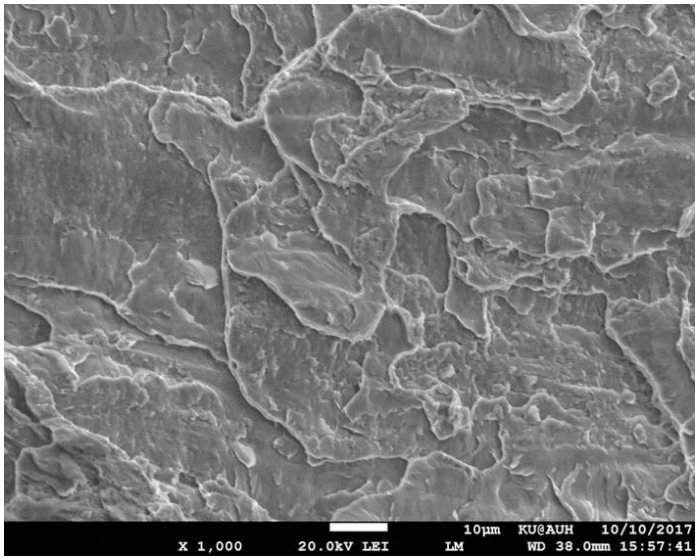

Figure 45. Cleavage fracture in SOHIC region between HIC cracks.

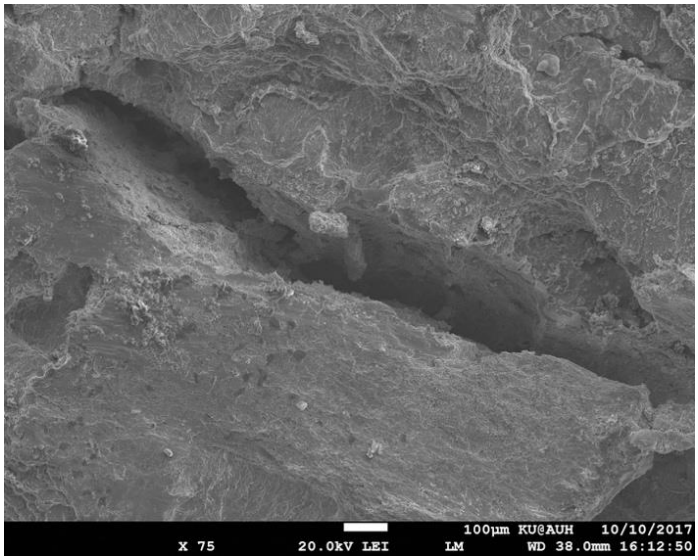

Figure 46. A large HIC crack at the SOHIC fracture region.

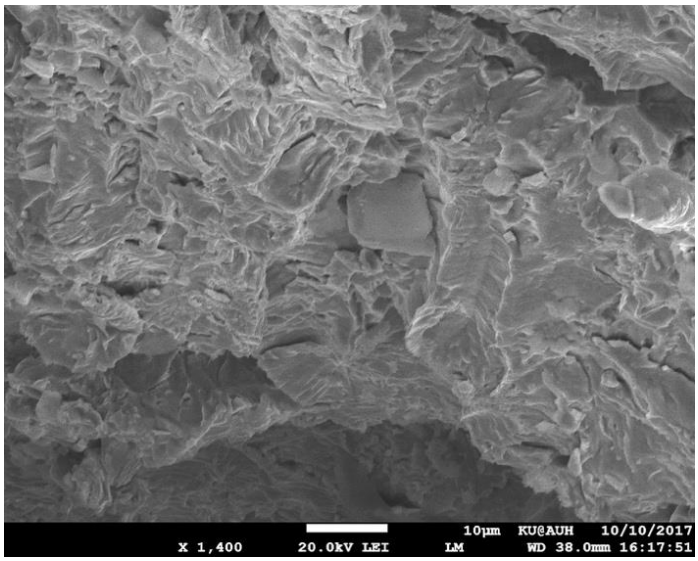

Figure 47. Cleavage fracture morphology of the internal blister/HIC crack wall.

It is important to note that location 577 exhibited only stacked HIC cracks with no evidence of crack linking. This indicates that the SOHIC sequence involves the formation of HIC cracks first, followed by through thickness linking of the HIC cracks, in agreement with observations by Crolet and Adam [38] and Ohki et al. [39]. Both HIC formation and linking involve transgranular cleavage fracture mechanisms as indicated by the fractographic analysis of the opened crack at location 500. The transgranular propagation mode is in agreement with the findings of Bruckhoff et al. [40], however the cleavage mode of linking is not in agreement with the suggestion of Pargeter [6] that linking is through a slip mechanism or of Azevedo [41] who observed ductile fracture mode in linking hydrogen blisters in an API 5L X46 steel. Slip may be involved in the transport of hydrogen, as shown by several studies [42, 43] but the propagation of the linking cracks is clearly through a cleavage mechanism. The cleavage mode of the linking cracks confirms the important influence of stress triaxiality in SOHIC since triaxiality introduces plastic constraint and promotes cleavage fracture. Triaxiality effects have been discussed by other investigators, such as the effect on hydrogen concentration by Toribio et al. [44], the effect on ductility by Mirza et al. [45] and the effect on fracture behavior by Borvik et al. [46].

4.5 Implications for H_2S/ Amine Service

The results presented above indicated that the failure mechanism of the absorber column, which operated under wet H_2S conditions, was SOHIC. The main characteristic of SOHIC is the presence of HIC cracks lying on the rolling plane, stacked one on top of the other and linked with cracks running perpendicular to the hoop stress. The SOHIC sequence involves the formation of HIC cracks first, followed by through thickness linking of the HIC cracks. The major contributing factors have been: (a) high hydrogen charging conditions, since for some time periods the vessel operated under high H2S/MDEA ratios, (b) stress triaxiality, imposed by the relatively large thickness of the plate. The role of these two factors have been discussed thoroughly above. An additional factor that may have to be considered is the type of steel used for the construction of the vessel. As discussed in the review by Ossai et al. [47] there is a need for high quality steel, free from inclusions and other microstructural defects that could act as sites for hydrogen related crack initiation. For wet H2S service it is typical to use a HIC-resistant steel. However, as indicated by the resulting cracking, a HIC-resistant steel might not be SOHIC-resistant in particular when subjected to high hydrogen charging conditions. This argument has also been raised by Pargeter [6]. As mentioned above, inclusions could act as potential sites for HIC. It appears that clean steels, such as the HIC-resistant steels, contain fewer stringer-type inclusions than conventional steels. In these cases, HIC is rather initiated on other interfaces, such as ferrite-pearlite interfaces. The metallographic analysis at the 577-position revealed that HIC cracks propagate in the ferrite matrix between pearlite colonies, as also observed in [48]. It is apparent that the use of a HIC-resistant steel should not be the only measure for mitigating SOHIC. Current practice in the fabrication of pressure vessels, operating in similar environment, calls for the use of austenitic stainless-steel lining, in order to reduce hydrogen diffusion and hydrogen entry to the steel plate. In

addition, operating conditions should be carefully monitored to minimize service under high H2S /amine ratios.

Finally, it is important to note that the results of mechanical testing indicated that the ductility of the steel, in regions away from the observed cracking has not deteriorated. Tensile elongation and notch ductility were maintained at high levels. However, even in a highly localized form, SOHIC did take place, indicating the type of hydrogen damage that can take place in an otherwise ductile material.

5 Conclusions

Taking into account the results presented above, the following conclusions can be drawn:

(1) The cracking in the amine absorber column shell is classified as stress-oriented hydrogen induced cracking (SOHIC).

(2) SOHIC proceeds in two steps: (a) initiation of small HIC cracks lying in the rolling plane and stacked in a direction normal to the applied stress, (b) through thickness linking of HIC cracks.

(3) The propagation of the HIC cracks as well as the through-thickness link cracks is associated to cleavage fracture mechanisms.

(4) The key factors identified in this failure were: (a) short periods of high hydrogen charging conditions as manifested by high H_2S/MDEA ratios and (b) stress triaxiality imposed by the relatively large thickness of the plate.

(5) The results indicate that a HIC-resistant steel might not be immune from SOHIC. Under high hydrogen charging conditions HIC cracks can initiate at interfaces other than stringer-type inclusions, such as ferrite/pearlite interfaces in the microstructure of the steel.

6 Appendix A

The stresses in the shell of a thick-wall cylindrical vessel subjected to an internal pressure are

$$\sigma_z = (p_i r_i^2 - p_o r_o^2) / (r_o^2 - r_i^2)$$

$$\sigma_\theta = [(p_i r_i^2 - p_o r_o^2) / (r_o^2 - r_i^2)] - [r_i^2 r_o^2 (p_o - p_i) / (r^2 (r_o^2 - r_i^2))]$$

$$s_r = [(p_i r_i^2 - p_o r_o^2) / (r_o^2 - r_i^2)] + [r_i^2 r_o^2 (p_o - p_i) / (r^2 (r_o^2 - r_i^2))]$$

where σ_z, σ_ϑ and σ_r are the axial, circumferential (hoop) and radial stresses respectively, p_i and p_o are the internal and external pressures, r_i and r_o are the internal and external radii of the cylinder. Inserting p_i=8 MPa, p_o=0.1MPa, r_i=1100mm and r_o=1191mm, then at position r=1110mm, i.e., 10mm from the internal surface, the stresses are σ_z=45.8 MPa, σ_ϑ=98.5 MPa and σ_r=-7 MPa. Stress triaxiality is defined by the ratio $s_h / \bar{s}$, where s_h is the hydrostatic stress and $\bar{s}$ is the Von-Mises equivalent stress given by:

$$\sigma_h = \frac{1}{3}(\sigma_z + \sigma_\theta + \sigma_r)$$

$$\bar{\sigma} = \sqrt{\frac{1}{2}[(\sigma_z - \sigma_\theta)^2 + (\sigma_\theta - \sigma_r)^2 + (\sigma_r - \sigma_z)^2]}$$

Inserting the above values for stresses, the triaxiality ratio is derived as $s_h / \bar{s} = 0.5$.

7 References

1. Kh., M., et al., *AMINE ABSORPTION COLUMN DESIGN USING MASS TRANSFER RATE SIMULATION*. 2005.
2. *Damage mechanisms affecting fixed equipment in the refining and petrochemical industries*, in *API RP 571*. 2011, American Petroleum Institute: Washington, D.C.
3. *Guidelines on Materials Requirements for Carbon and Low Alloy Steels for H2S Containing Environments in Oil and Gas Production*.
4. *Fittness-for-service*. 2007, American Petroleum Institute: Washington, D.C.
5. Buchheim, G.M., D.A. Osage, and J.C. Staats, *Development of Fitness-for-Service Rules for the Assessment of HIC and SOHIC Damage in API 579-1/ASME FFS-1.* 2008: p. 761-775.
6. Pargeter, R.J., *Susceptibility to SOHIC for linepipe and pressure vessel steels - review of current knowledge*, in *NACE 2007*. 2007: Nashville, Tennessee.
7. McHenry, H.I., et al., *Examination of a pressure vessel that ruptured at the Chicago refinery of the Union Oil Company on July 23 1984*, U.D.o.L. Occupational Safety & Health Administration, Editor. 1986.
8. Al-Anezi, M.A. and S. Rao, *Failures by SOHIC in Sour Hydrocarbon Service.* Journal of Failure Analysis and Prevention, 2011. **11**(4): p. 363-371.
9. Kobayashi, K., P. Dent, and C.M. Fowler, *Effects of Stress Conditions and Microstructure on SOHIC Susceptibility*, in *CORROSION 2014*. 2014, NACE International: San Antonio, Texas, USA.
10. Koh, S.U., et al., *Effect of Microstructure on Hydrogen-Induced Cracking of Linepipe Steels.* CORROSION, 2008. **64**(7): p. 574-585.
11. Tsuchida, Y., Y. Naruoka, and Y. Tokunaga, *Effects of Heat Treatment Conditions on SOHIC in Normalized Steel Plates for Pressure Vessel Use.* Journal of High Pressure Institute of Japan, 1996. **34**(1): p. 9-15.
12. Findley, K.O., M.K. O'Brien, and H. Nako, *Critical Assessment 17: Mechanisms of hydrogen induced cracking in pipeline steels.* Materials Science and Technology, 2015. **31**(14): p. 1673-1680.
13. Gan, L., et al., *Hydrogen trapping and hydrogen induced cracking of welded X100 pipeline steel in H_2S environments.* International Journal of Hydrogen Energy, 2018. **43**(4): p. 2293-2306.
14. Fujishiro, M.T. and D.T. Hara, *In-situ observation of Hydrogen Induced Cracking propagation behavior.* CORROSION: p. in print.
15. Okonkwo, P., et al., *Corrosion Behavior of API X100 Steel Material in a Hydrogen Sulfide Environment.* Metals, 2017. **7**(4): p. 109.
16. Ghosh, G., et al., *Hydrogen induced cracking of pipeline and pressure vessel steels: A review.* Engineering Fracture Mechanics, 2018. **199**: p. 609-618.
17. Mitra, S., *A technical report on gas sweetening system*. 2015.
18. Kane, R.D., *"Roles of H2S in the Behavior of Engineering Alloys", Corrosion/98*, N. International, Editor. 1998.
19. Kane, R.D., *Roles of H2S in behaviour of engineering alloys.* International Metals Reviews, 1985. **30**(1): p. 291-301.

20. Groysman, A., *Corrosion problems and solutions in oil refining and petrochemical Industry*, in *Topics in safety, risk, reliability and quality v 32*. 2017, Springer,: Cham. p. 1 online resource (369 p.
21. Zheng, C., et al., *Hydrogen permeation behavior and corrosion monitoring of steel in cyclic wet–dry atmospheric environment.*
22. Andersen, J.B., et al., *Design and Installation of Marine Pipelines*. 2005.
23. M., E., *HYDROGEN-INDUCED CRACKING AND SULFIDE STRESS CRACKING*, in *Uhlig Corrosion Handbook*. 2011.
24. Augusto, S., *MECHANICAL BEHAVIOUR OF HIGH TOUGHNESS STEELS IN EXTREME ENVIRONMENTS: INFLUENCE OF HYDROGEN AND LOW TEMPERATURE*. 2011, University Of Milano.
25. Zhao, M.C., et al., *Role of microstructure on sulfide stress cracking of oil and gas pipeline steels.* Metallurgical and Materials Transactions a-Physical Metallurgy and Materials Science, 2003. 34a(5): p. 1089-1096.
26. Beke, L., *Contamination in Amine Systems*

2010.
27. Liu, H.J., J.W. Dean, and S.F. Bosen, *Neutralization Technology to Reduce Corrosion from Heat Stable Amine Salts*, N. International, Editor. 1995.
28. *Standard Specification for Pressure Vessel Plates, Carbon Steel, for Moderate- and Lower- Temperature Service*. 2008.
29. *Evaluation of pipeline and pressure vessel steels for resistance to hydrogen-induced cracking*, in *NACE standard TM-0284-2003*. 2003, NACE International: Houston, Texas.
30. American Society for Metals., ASM International. Handbook Committee., and Knovel (Firm), *ASM handbook. Volume 10, Materials characterization*. 1986, American Society for Metals.: Metals Park, Ohio. p. xi, 761 p.
31. *ASM HANDBOOK*.
32. Kelkar, K.M., et al., *Computational Modeling of the Vacuum Arc Remelting (VAR) Process Used for the Production of Ingots of Titanium Alloys*. 2019.
33. Vander Voort, G.F., *Metallography, principles and practice*. 1999, ASM International,: Materials Park, OH. p. 1 online resource (xiv, 752 p.
34. ASM International. Handbook Committee. and Knovel (Firm), *ASM handbook. Volume 8, Mechanical testing and evaluation*. 2000, ASM International,: Materials Park, OH. p. xiv, 998 p.
35. American Society for Metals., ASM International. Handbook Committee., and Knovel (Firm), *ASM handbook. Volume 12, Fractography*. 1987, American Society for Metals.: Metals Park, Ohio. p. xiii, 517 p.
36. Gingell, A. and X. Garat. *Observations of Damage Modes as a Function of Microstructure During NACE TM-01-77/96 Tensile Testing of API 5L Grade X60 Linepipe Steels*. in *CORROSION 99*. 1999. San Antonio, Texas: NACE International.
37. .
38. Crolet, J.L. and C. Adam, *SOHIC without H_2S.* Materials Performance, 2000. 39(3): p. 86-90.
39. Ohki, T., et al. *Effect of inclusions on sulphide stress cracking*. in *Symposium on Stress Corrosion - New Approaches*. Montreal, Canada.

40. Bruckhoff, W., et al. *Rupture of a sour gas line due to Stress Orientated Hydrogen Induced Cracking - Failure analyses, experimental results and corrosion prevention*. in *NACE CORROSION/85*. Boston, Massachusetts, USA.
41. Azevedo, C.R.F., *Failure analysis of a crude oil pipeline.* Engineering Failure Analysis, 2007. **14**(6): p. 978-994.
42. Miyoshi, E., et al., *Hydrogen-Induced Cracking of Steels under Wet Hydrogen-Sulfide Environment.* Journal of Engineering for Industry, 1976. **98**(4): p. 1221-1230.
43. Robertson, I.M., et al., *Hydrogen Embrittlement Understood.* Metallurgical and Materials Transactions B, 2015. **46**(3): p. 1085-1103.
44. Toribio, J., et al., *Hydrogen Diffusion in Metals Assisted by Stress: 2D Numerical Modelling and Analysis of Directionality.* Solid State Phenomena, 2015. **225**: p. 33-38.
45. Mirza, M.S., D.C. Barton, and P. Church, *The effect of stress triaxiality and strain-rate on the fracture characteristics of ductile metals.* Journal of Materials Science, 1996. **31**(2): p. 453-461.
46. Børvik, T., O.S. Hopperstad, and T. Berstad, *On the influence of stress triaxiality and strain rate on the behaviour of a structural steel. Part II. Numerical study.* European Journal of Mechanics - A/Solids, 2003. **22**(1): p. 15-32.
47. Ossai, C.I., B. Boswell, and I.J. Davies, *Pipeline failures in corrosive environments - A conceptual analysis of trends and effects.* Engineering Failure Analysis, 2015. **53**: p. 36-58.
48. Cayard, M.S., R.D. Kane, and D.L. Cooke, *An Exploratory Examination Of The Effect Of Sohic Damage On The Fracture Resistance Of Carbon Steels*, in *CORROSION 97*. 1997, NACE International: New Orleans, Louisiana.